Approximate analysis of three-dimensional groundwater flow toward a radial collector well in a finite-extent unconfined aquifer

Ching-Sheng Huang[1], Jyun-Jie Chen[1], and Hund-Der Yeh[1*]

Submitted to *Hydrology and Earth System Sciences* **on June 14, 2015**

Re-submitted to *Hydrology and Earth System Sciences* **on July 22, 2015**

Re-re-submitted to *Hydrology and Earth System Sciences* **on October 14, 2015**

[1] Institute of Environmental Engineering, National Chiao Tung University, Hsinchu, Taiwan.

*** Corresponding Author**

Address: Institute of Environmental Engineering, National Chiao Tung University, 1001 University Road, Hsinchu 300, Taiwan

E-mail address: hdyeh@mail.nctu.edu.tw; Tel: 886-3-5731910; Fax: 886-3-5725958

Abstract

This study develops a three-dimensional mathematical model for describing transient hydraulic head distributions due to pumping at a radial collector well (RCW) in a rectangular confined or unconfined aquifer bounded by two parallel streams and no-flow boundaries. The streams with low-permeability streambeds fully penetrate the aquifer thickness. The governing equation with a point-sink term is employed. A first-order free surface equation delineating the water table decline induced by the well is considered. Robin boundary conditions are adopted to describe fluxes across the streambeds. The head solution for the point sink is derived by applying the methods of finite integral transform and Laplace transform. The head solution for a RCW is obtained by integrating the point-sink solution along the laterals of the RCW and then dividing the integration result by the sum of lateral lengths. On the basis of Darcy's law and head distributions along the streams, the solution for the stream depletion rate (SDR) can also be developed. With the aid of the head and SDR solutions, the sensitivity analysis can then be performed to explore the response of the hydraulic head to the change in a specific parameter such as the horizontal and vertical hydraulic conductivities, streambed permeability, specific storage, specific yield, lateral length and well depth. Spatial head distributions subject to the anisotropy of aquifer hydraulic conductivities are analyzed. A quantitative criterion is provided to identify whether groundwater flow at a specific region is 3-D or 2-D without the vertical component. In addition, another criterion is also given to allow the neglect of vertical flow effect on SDR. Conventional 2-D flow models can be used to provide accurate head and SDR predictions if satisfying these two criteria.

Keywords: Robin boundary condition, sensitivity analysis, stream depletion rate, first-order free surface equation, analytical solution

1. Introduction

The applications of a radial collector well (RCW) have received much attention in the aspects of water resource supply and groundwater remediation since rapid advances in drilling technology. An average yield for the well approximates 27,000 m^3/day (Todd and Mays, 2005). As compared to vertical wells, RCWs require less operating cost, produce smaller drawdown, and have better efficiency of withdrawing water from thin aquifers. In addition, RCWs can extract water from an aquifer underlying obstacles such as buildings, but vertical wells cannot. Recently, Huang et al. (2012) reviewed semi-analytical and analytical solutions associated with RCWs. Since then, Yeh and Chang (2013) provided a valuable overview of articles associated with RCWs.

A variety of analytical models involving a horizontal well, a specific case of a RCW with a single lateral, in aquifers were developed (e.g., Park and Zhan, 2003; Hunt, 2005; Anderson, 2013). The flux along the well screen is commonly assumed to be uniform. The equation describing three-dimensional (3-D) flow is used. Kawecki (2000) developed analytical solutions of the hydraulic heads for the early linear flow perpendicular to a horizontal well and late pseudo-radial flow toward the middle of the well in confined aquifers. They also developed an approximate solution for unconfined aquifers on the basis of the head solution and an unconfined flow modification. The applicability of the approximate solution was later evaluated in comparison with a finite difference solution developed by Kawecki and Al-Subaikhy (2005). Zhan et al. (2001) presented an analytical solution for drawdown induced by a horizontal well in confined aquifers and compared the difference in the type curves based on the well and a vertical well. Zhan and Zlotnik (2002) developed a semi-analytical solution of drawdown due to pumping from a nonvertical well in an unconfined aquifer accounting for the effect of instantaneous drainage or delayed yield when the free surface declines. They discussed the influences of the length, depth, and inclination of the well on temporal drawdown

distributions. Park and Zhan (2002) developed a semi-analytical drawdown solution considering the effects of a finite diameter, the wellbore storage, and a skin zone around a horizontal well in anisotropic leaky aquifers. They found that those effects cause significant change in drawdown at an early pumping period. Zhan and Park (2003) provided a general semi-analytical solution for pumping-induced drawdown in a confined aquifer, an unconfined aquifer on a leaky bottom, or a leaky aquifer below a water reservoir. Temporal drawdown distributions subject to the aquitard storage effect were compared with those without that effect. Sun and Zhan (2006) derived a semi-analytical solution of drawdown due to pumping at a horizontal well in a leaky aquifer. A transient one-dimensional flow equation describing the vertical flow across the aquitard was considered. The derived solution was used to evaluate the Zhan and Park (2003) solution which assumed steady-state vertical flow in the aquitard.

Sophisticated numerical models involved in RCWs or horizontal wells were also reported. Steward (1999) applied the analytic element method to approximate 3-D steady-state flow induced by horizontal wells in contaminated aquifers. They discussed the relation between a pumping rate and the size of a polluted area. Chen et al. (2003) utilized the polygon finite difference method to deal with three kinds of seepage-pipe flows including laminar, turbulent, and transitional flows within a finite-diameter horizontal well. A sandbox experiment was also carried out to verify the prediction made by the method. Mohamad and Rushton (2006) used MODFLOW to predict flows inside an aquifer, from the aquifer to a horizontal well, and within the well. The predicted head distributions were compared with field data measured in Sarawak, Malaysia. Su et al. (2007) used software TOUGH2 based on the integrated finite difference method to handle irregular configurations of several laterals of two RCWs installed beside the Russian River, Forestville, California and analyzed pumping-induced unsaturated regions beneath the river. Lee et al. (2012) developed a finite element solution with triangle elements to assess whether the operation of a RCW near Nakdong River in South Korea can induce

92 riverbank filtration. They concluded that the well can be used for sustainable water supply at
93 the study site. In addition, Rushton and Brassington (2013a) extended Mohamad and Rushton
94 (2006) study by enhancing the Darcy-Weisbach formula to describe frictional head lose inside
95 a horizontal well. The spatial distributions of predicted flux along the well revealed that the
96 flux at the pumping end is four times of the magnitude of that at the far end. Later, Rushton
97 and Brassington (2013b) applied the same model to a field experiment at the Seton Coast,
98 northwest England.

99 Well pumping in aquifers near streams may cause groundwater−surface water interactions
100 (e.g., Rodriguez et al., 2013; Chen et al., 2013; Zhou et al., 2013; Exner-Kittridge et al., 2014;
101 Flipo et al., 2014; Unland et al., 2014). The stream depletion rate (SDR), commonly used to
102 quantify stream water filtration into the adjacent aquifer, is defined as the ratio of the filtration
103 rate to a pumping rate. The SDR ranges from zero to a certain value which could be equal to
104 or less than unity (Zlotnik, 2004). Tsou et al. (2010) developed an analytical solution of SDR
105 for a slanted well in confined aquifers adjacent to a stream treated as a constant-head boundary.
106 They indicated that a horizontal well parallel to the stream induces the steady-state SDR of
107 unity more quickly than a slanted well. Huang et al. (2011) developed an analytical SDR
108 solution for a horizontal well in unconfined aquifers near a stream regarded as a constant-head
109 boundary. Huang et al. (2012) provided an analytical solution for SDR induced by a RCW in
110 unconfined aquifers adjacent to a stream with a low-permeability streambed treated as the
111 Robin condition. The influence of the configuration of the laterals on temporal SDR and spatial
112 drawdown distributions was analyzed. Recently, Huang et al. (2014) gave an exhaustive review
113 on analytical and semi-analytical SDR solutions and classified these solutions into two
114 categories. One group involved two-dimensional (2-D) flow toward a fully-penetrating vertical
115 well according to aquifer types and stream treatments. The other group included the solutions
116 involving 3-D and quasi 3-D flows in the lights of aquifer types, well types, and stream

117 treatments.

118 At present, existing analytical solutions associated with flow toward a RCW in unconfined
119 aquifers have involved laborious calculation (Huang et al., 2012) and predicted approximate
120 results (Hantush and Papadopoulos, 1962). The Huang et al. (2012) solution involves numerical
121 integration of a triple integral in predicting the hydraulic head and a quintuple integral in
122 predicting SDR. The integrand is expressed in terms of an infinite series expanded by roots of
123 nonlinear equations. The integration variables are related to those roots. The application of
124 their solution is therefore limited to those who are familiar with numerical methods. In addition,
125 the accuracy of the Hantush and Papadopoulos (1962) solution is limited to some parts of a
126 pumping period; that is, it gives accurate drawdown predictions at early and late times but
127 divergent ones at middle time.

128 The objective of this study is to present new analytical solutions of the head and SDR,
129 which overcome the above−mentioned limitations, for 3-D flow toward a RCW. A
130 mathematical model is built to describe 3-D spatiotemporal hydraulic head distributions in a
131 rectangular unconfined aquifer bounded by two parallel streams and by the no-flow stratums
132 in the other two sides. The flux across the well screen is assumed to be uniform along each of
133 the laterals. The assumption is valid for a short lateral within 150 m verified by agreement on
134 drawdown observed in field experiments and predicted by existing analytical solutions (Huang
135 et al., 2011; 2012). The streams fully penetrate the aquifer thickness and connect the aquifer
136 with low-permeability streambeds. The model for the aquifer system with two parallel streams
137 can be used to determine the fraction of water filtration from the streams and solve the
138 associated water right problem (Sun and Zhan, 2007). The transient 3-D groundwater flow
139 equation with a point-sink term is considered. The first-order free surface equation is used to
140 describe water table decline due to pumping. Robin boundary conditions are adopted to
141 describe fluxes across the streambeds. The head solution for a point sink is derived by the

methods of Laplace transform and finite integral transform. The analytical head solution for a RCW is then obtained by integrating the point-sink solution along the well and dividing the integration result by the total lateral length. The RCW head solution is expressed in terms of a triple series expanded by eigenvalues which can be obtained by a numerical algorithm such as Newton's method. On the basis of Darcy's law and the RCW head solution, the SDR solution can then be obtained in terms of a double series with fast convergence. With the aid of both solutions, the sensitivity analysis is performed to investigate the response of the hydraulic head to the change in each of aquifer parameters. The spatial distributions of the head and streamline are discussed. Spatial head distributions subject to the anisotropy of aquifer hydraulic conductivities are analyzed. The influences of the vertical flow and well depth on temporal SDR distributions are investigated. Moreover, temporal SDR distributions induced by a RCW and a fully penetrating vertical well in confined aquifers are also compared. A quantitative criterion is provided to identify whether groundwater flow at a specific region is 3-D or 2-D without the vertical component. In addition, another criterion is also given to judge the suitability of neglecting the vertical flow effect on SDR.

2. Methodology

2.1. Mathematical model

Consider a RCW in a rectangular unconfined aquifer bounded by two parallel streams and no-flow stratums as illustrated in Figure 1. The symbols for variables and parameters are defined in Table 1. The origin of the Cartesian coordinate is located at the lower left corner. The aquifer domain falls in the range of $0 \le x \le w_x$, $0 \le y \le w_y$, and $-H \le z \le 0$. The RCW consists of a caisson and several laterals, each of which extends finitely with length L_k and counterclockwise with angle θ_k where $k \in 1, 2, \ldots N$ and N is the number of laterals. The caisson is located at (x_0, y_0), and the surrounding laterals are at $z = -z_0$.

First of all, a mathematical model describing 3-D flow toward a point sink in the aquifer is proposed. The equation describing 3-D hydraulic head distribution $h(x, y, z, t)$ is expressed as

$$K_x \frac{\partial^2 h}{\partial x^2} + K_y \frac{\partial^2 h}{\partial y^2} + K_z \frac{\partial^2 h}{\partial z^2} = S_s \frac{\partial h}{\partial t} + Q\,\delta(x - x_0')\delta(y - y_0')\delta(z + z_0') \quad (1)$$

where $\delta(\ )$ is the Dirac delta function, the second term on the right-hand side (RHS) indicates the point sink, and Q is positive for pumping and negative for injection. The first term on the RHS of Eq. (1) depicts aquifer storage release based on the concept of effective stress proposed by Terzaghi (see, for example, Bear, 1979; Charbeneau, 2000), which is valid under the assumption of constant total stress. By choosing water table as a reference datum where the elevation head is set to zero, the initial condition can therefore be denoted as

$$h = 0 \quad \text{at} \quad t = 0 \quad (2)$$

Note that equation (2) introduces negative hydraulic head for pumping, and the absolute value of the head equals drawdown.

The aquifer boundaries at $x = 0$ and $x = w_x$ are considered to be impermeable and thus expressed as

$$\partial h / \partial x = 0 \quad \text{at} \quad x = 0 \quad (3)$$

and

$$\partial h / \partial x = 0 \quad \text{at} \quad x = w_x \quad (4)$$

Streambed permeability is usually less than the adjacent aquifer formation. The fluxes across the streambeds can be described by Robin boundary conditions as

$$K_y \frac{\partial h}{\partial y} - \frac{K_1}{b_1} h = 0 \quad \text{at} \quad y = 0 \quad (5)$$

and

$$K_y \frac{\partial h}{\partial y} + \frac{K_2}{b_2} h = 0 \quad \text{at} \quad y = w_y \quad (6)$$

190 The free surface equation describing water table decline is written as

191 $$K_x\left(\frac{\partial h}{\partial x}\right)^2 + K_y\left(\frac{\partial h}{\partial y}\right)^2 + K_z\left(\frac{\partial h}{\partial z}\right)^2 - K_z\frac{\partial h}{\partial z} = S_y\frac{\partial h}{\partial t} \quad \text{at} \quad z = h \tag{7}$$

192 Neuman (1972) indicated that the effect of the second-order terms in Eq. (7) is generally
193 ignorable to develop analytical solutions. Eq. (7) is thus linearized by neglecting the quadratic
194 terms, and the position of the water table is fixed at the initial condition (i.e., $z = 0$). The result
195 is written as

196 $$K_z\frac{\partial h}{\partial z} = -S_y\frac{\partial h}{\partial t} \quad \text{at} \quad z = 0 \tag{8}$$

197 Notice that Eq. (8) is applicable when the conditions $|h|/H \leq 0.1$ and $|\partial h/\partial x| +$
198 $|\partial h/\partial y| \leq 0.01$ are satisfied. These two conditions had been studied and verified by
199 simulations in, for example, Nyholm et al. (2002), Goldscheider and Drew (2007) and Yeh et
200 al. (2010). Nyholm et al. (2002) achieved agreement on drawdown measured in a field pumping
201 test and predicted by MODFLOW which models flow in the study site as confined behavior
202 because of $|h|/H \leq 0.1$ in the pumping well. Goldscheider and Drew (2007) revealed that
203 pumping drawdown predicted by Neuman (1972) analytical solution based on Eq. (8) agrees
204 well with that obtained in a field pumping test. In addition, Yeh et al. (2010) also achieved
205 agreement on the hydraulic head predicted by their analytical solution based on Eq. (8), their
206 finite difference solution based on Eq. (7) with $\partial h/\partial y = 0$ (referring to Eq. (7a)), and Teo et
207 al. (2003) solution derived by applying the perturbation technique to deal with Eq. (7a) when
208 $|h|/H = 0.1$ and $|\partial h/\partial x| = 0.01$ (i.e., $\alpha = 0.1$ and $|\partial\phi/\partial x| = 0.01$ at $x = 0$ in Yeh et al.
209 (2010, Fig. 5(a)). On the other hand, the bottom of the aquifer is considered as a no-flow
210 boundary condition denoted as

211 $$\partial h/\partial z = 0 \quad \text{at} \quad z = -H \tag{9}$$

212 Define dimensionless variables as $\bar{h} = (K_y\, H\, h)/Q$, $\bar{t} = (K_y\, t)/(S_s\, y_0^2)$, $\bar{x} = x/y_0$,

$\bar{y} = y/y_0$, $\bar{z} = z/H$, $\bar{x}_0' = x_0'/y_0$, $\bar{y}_0' = y_0'/y_0$, $\bar{z}_0' = z_0'/H$, $\bar{w}_x = w_x/y_0$ and $\bar{w}_y = w_y/y_0$ where the overbar denotes a dimensionless symbol, and y_0, a distance between stream 1 and the center of the RCW, is chosen as a characteristic length. On the basis of the definitions, Eq. (1) can be written as

$$\kappa_x \frac{\partial^2 \bar{h}}{\partial \bar{x}^2} + \frac{\partial^2 \bar{h}}{\partial \bar{y}^2} + \kappa_z \frac{\partial^2 \bar{h}}{\partial \bar{z}^2} = \frac{\partial \bar{h}}{\partial \bar{t}} + \delta(\bar{x} - \bar{x}_0')\delta(\bar{y}' - \bar{y}_0')\delta(\bar{z} + \bar{z}_0') \tag{10}$$

where $\kappa_x = K_x/K_y$ and $\kappa_z = (K_z\, y_0^2)/(K_y\, H^2)$.

Similarly, the initial and boundary conditions are expressed as

$$\bar{h} = 0 \quad \text{at} \quad \bar{t} = 0 \tag{11}$$

$$\partial \bar{h}/\partial \bar{x} = 0 \quad \text{at} \quad \bar{x} = 0 \tag{12}$$

$$\partial \bar{h}/\partial \bar{x} = 0 \quad \text{at} \quad \bar{x} = \bar{w}_x \tag{13}$$

$$\partial \bar{h}/\partial \bar{y} - \kappa_1 \bar{h} = 0 \quad \text{at} \quad \bar{y} = 0 \tag{14}$$

$$\partial \bar{h}/\partial \bar{y} + \kappa_2 \bar{h} = 0 \quad \text{at} \quad \bar{y} = \bar{w}_y \tag{15}$$

$$\frac{\partial \bar{h}}{\partial \bar{z}} = -\frac{\gamma}{\kappa_z}\frac{\partial \bar{h}}{\partial \bar{t}} \quad \text{at} \quad \bar{z} = 0 \tag{16}$$

and

$$\partial \bar{h}/\partial \bar{z} = 0 \quad \text{at} \quad \bar{z} = -1 \tag{17}$$

where $\kappa_1 = (K_1\, y_0)/(K_y\, b_1)$, $\kappa_2 = (K_2\, y_0)/(K_y\, b_2)$ and $\gamma = S_y/(S_s\, H)$.

2.2 Head solution for point sink

The model, Eqs. (10) – (17), reduces to an ordinary differential equation (ODE) with two boundary conditions in terms of $\bar{z}$ after taking Laplace transform and finite integral transform. The former transform converts $\bar{h}(\bar{x}, \bar{y}, \bar{z}, \bar{t})$ into $\hat{h}(\bar{x}, \bar{y}, \bar{z}, p)$, $\delta(\bar{x} - \bar{x}_0')\, \delta(\bar{y} - \bar{y}_0')\delta(\bar{z} - \bar{z}_0')$ in Eq. (10) into $\delta(\bar{x} - \bar{x}_0')\, \delta(\bar{y} - \bar{y}_0')\delta(\bar{z} - \bar{z}_0')/p$, and $\partial \bar{h}/\partial \bar{t}$ in Eqs. (10) and (16) into $p\hat{h} - \bar{h}\big|_{\bar{t}=0}$ where p is the Laplace parameter, and the second term, initial condition in Eq. (11),

equals zero (Kreyszig, 1999). The transformed model becomes a boundary value problem written as

$$\kappa_x \frac{\partial^2 \hat{h}}{\partial \bar{x}^2} + \frac{\partial^2 \hat{h}}{\partial \bar{y}^2} + \kappa_z \frac{\partial^2 \hat{h}}{\partial \bar{z}^2} = p\hat{h} + \delta(\bar{x} - \bar{x}_0')\delta(\bar{y}' - \bar{y}_0')\delta(\bar{z} + \bar{z}_0')/\, p \tag{18}$$

with boundary conditions $\partial \hat{h}/\, \partial \bar{x} = 0$ at $\bar{x} = 0$ and $\bar{x} = \bar{w}_x$, $\partial \hat{h}/\partial \bar{y} - \kappa_1 \hat{h} = 0$ at $\bar{y} = 0$, $\partial \hat{h}/\partial \bar{y} + \kappa_2 \hat{h} = 0$ at $\bar{y} = \bar{w}_y$, $\partial \hat{h}/\partial \bar{z} = -p\gamma \hat{h}/\kappa_z$ at $\bar{z} = 0$ and $\partial \bar{h}/\partial \bar{z} = 0$ at $\bar{z} = -1$. We then apply finite integral transform to the problem. One can refer to Appendix A for its detailed definition. The transform converts $\hat{h}(\bar{x}, \bar{y}, \bar{z}, p)$ in the problem into $\tilde{h}(\alpha_m, \beta_n, \bar{z}, p)$, and $\delta(\bar{x} - \bar{x}_0')\, \delta(\bar{y} - \bar{y}_0')$ in Eq. (18) into $\cos(\alpha_m \bar{x}_0') K(\bar{y}_0')$ and $\kappa_x\, \partial^2 \hat{h}/\partial \bar{x}^2 + \partial^2 \hat{h}/\partial \bar{y}^2$ in Eq. (18) into $-(\kappa_x \alpha_m^2 + \beta_n^2)\tilde{h}$ where $(m,\, n) \in 1,\, 2,\, 3,\, \ldots\, \infty$, $\alpha_m = m\, \pi/\bar{w}_x$, $K(\bar{y}_0')$ is defined in Eq. (A2) with $\bar{y} = \bar{y}_0'$, and β_n are eigenvalues equaling the roots of the following equation as (Latinopoulos, 1985)

$$\tan\left(\beta_n\, \bar{w}_y\right) = \frac{\beta_n(\kappa_1 + \kappa_2)}{\beta_n^2 - \kappa_1\, \kappa_2} \tag{19}$$

The method to determine the roots is discussed in section 2.3. In turn, Eq. (18) becomes a second-order ODE defined by

$$\kappa_z \frac{\partial^2 \tilde{h}}{\partial \bar{z}^2} - (\kappa_x \alpha_m^2 + \beta_n^2 + p)\tilde{h} = \cos(\alpha_m\, \bar{x}_0')\, K(\bar{y}_0')\, \delta(\bar{z} + \bar{z}_0')/\, p \tag{20}$$

with two boundary conditions denoted as

$$\frac{\partial \tilde{h}}{\partial \bar{z}} = -\frac{p\ \gamma}{\kappa_z} \tilde{h} \quad \text{at} \quad \bar{z} = 0 \tag{21}$$

and

$$\partial \tilde{h}/\partial \bar{z} = 0 \quad \text{at} \quad \bar{z} = -1 \tag{22}$$

Eq. (20) can be separated into two homogeneous ODEs as

$$\kappa_z \frac{\partial^2 \tilde{h}_a}{\partial \bar{z}^2} - (\kappa_x \alpha_m^2 + \beta_n^2 + p)\tilde{h}_a = 0 \quad \text{for} \quad -\bar{z}_0' \le \bar{z} \le 0 \tag{23}$$

and

$$\kappa_z \frac{\partial^2 \tilde{h}_b}{\partial \bar{z}^2} - (\kappa_x \alpha_m^2 + \beta_n^2 + p)\tilde{h}_b = 0 \quad \text{for} \quad -1 \le \bar{z} \le -\bar{z}_0' \tag{24}$$

where h_a and h_b, respectively, represent the heads above and below $\bar{z} = -\bar{z}_0'$ where the point sink is located. Two continuity requirements should be imposed at $\bar{z} = -\bar{z}_0'$. The first is the continuity of the hydraulic head denoted as

$$\tilde{h}_a = \tilde{h}_b \quad \text{at} \quad \bar{z} = -\bar{z}_0' \tag{25}$$

The second describes the discontinuity of the flux due to point pumping represented by the Dirac delta function in Eq. (20). It can be derived by integrating Eq. (20) from $\bar{z} = -\bar{z}_0'^{-}$ to $\bar{z} = -\bar{z}_0'^{+}$ as

$$\frac{\partial \tilde{h}_a}{\partial \bar{z}} - \frac{\partial \tilde{h}_b}{\partial \bar{z}} = \frac{\cos(\alpha_m \bar{x}_0') K(\bar{y}_0')}{p \kappa_z} \quad \text{at} \quad \bar{z} = -\bar{z}_0' \tag{26}$$

Solving Eqs. (23) and (24) simultaneously with Eqs. (21), (22), (25), and (26) yields the Laplace-domain head solution as

$$\tilde{h}_a(\alpha_m, \beta_n, \bar{z}, p) = \Omega(-\bar{z}_0', \bar{z}, 1) \quad \text{for} \quad -\bar{z}_0' \le \bar{z} \le 0 \tag{27a}$$

and

$$\tilde{h}_b(\alpha_m, \beta_n, \bar{z}, p) = \Omega(\bar{z}, \bar{z}_0', -1) \quad \text{for} \quad -1 \le \bar{z} \le -\bar{z}_0' \tag{27b}$$

with

$$\Omega(a,b,c) = \frac{\cosh[(1+a)\lambda][-\kappa_z \lambda \cosh(b\lambda) + c\, p\gamma \sinh(b\lambda)]\cos(\alpha_m \bar{x}_0) K(\bar{y}_0)}{p \kappa_z \lambda (p\gamma \cosh\lambda + \kappa_z \lambda \sinh\lambda)} \tag{28}$$

$$\lambda = \sqrt{(\kappa_x \alpha_m^2 + \beta_n^2 + p)/\kappa_z} \tag{29}$$

where a, b, and c are arguments. Taking the inverse Laplace transform and finite integral transform to Eq. (28) results in Eq. (31). One is referred to Appendix B for the detailed derivation. A time-domain head solution for a point sink is therefore written as

$$\bar{h}(\bar{x}, \bar{y}, \bar{z}, \bar{t}) = \begin{cases} \Phi(-\bar{z}_0', \bar{z}, 1) \text{ for } -\bar{z}_0' \le \bar{z} \le 0 \\ \Phi(\bar{z}, \bar{z}_0', -1) \text{ for } -1 \le \bar{z} \le -\bar{z}_0' \end{cases} \tag{30}$$

with

$$\Phi(a,b,c)=\frac{2}{\bar{w}_x}\left\{\sum_{n=1}^{\infty}\left[\phi_n X_n+2\sum_{m=1}^{\infty}\phi_{m,n}X_{m,n}\cos(\alpha_m\bar{x})\right]Y_n\right\} \tag{31}$$

$$\phi_{m,n}=\psi_{m,n}+\psi_{m,n,0}+\sum_{i=1}^{\infty}\psi_{m,n,i} \tag{32}$$

$$\psi_{m,n}=-\cosh[(1+a)\lambda_s]\cosh(b\,\lambda_s)/(\kappa_z\,\lambda_s\,\sinh\lambda_s) \tag{33}$$

$$\psi_{m,n,0}=\mu_{m,n,0}\cosh[(1+a)\lambda_0]\,[-\kappa_z\,\lambda_0\cosh(b\,\lambda_0)+c\,p_0\,\gamma\,\sinh(b\,\lambda_0)] \tag{34}$$

$$\psi_{m,n,i}=\nu_{m,n,i}\cos[(1+a)\lambda_i]\,[-\kappa_z\,\lambda_i\cos(b\,\lambda_i)+c\,p_i\,\gamma\,\sin(b\,\lambda_i)] \tag{35}$$

$$\mu_{m,n,0}=2\exp(p_0\,\bar{t})/\{p_0[(1+2\,\gamma)\,\kappa_z\,\lambda_0\cosh\lambda_0+(p_0\,\gamma+\kappa_z)\sinh\lambda_0]\} \tag{36}$$

$$\nu_{m,n,i}=2\exp(p_i\,\bar{t})/\{p_i[(1+2\,\gamma)\,\kappa_z\,\lambda_i\cos\lambda_i+(p_i\,\gamma+\kappa_z)\sin\lambda_i]\} \tag{37}$$

$$Y_n=\frac{\beta_n\cos(\beta_n\bar{y})+\kappa_1\sin(\beta_n\bar{y})}{(\beta_n^2+\kappa_1^2)[\bar{w}_y+\kappa_2/(\beta_n^2+\kappa_2^2)]+\kappa_1} \tag{38}$$

and

$$X_{m,n}=\cos(\alpha_m\bar{x}_0')\,[\beta_n\cos(\beta_n\bar{y}_0')+\kappa_1\sin(\beta_n\bar{y}_0')] \tag{39}$$

where $\lambda_s=\sqrt{(\kappa_x\alpha_m^2+\beta_n^2)/\kappa_z}$, $p_0=\kappa_z\lambda_0^2-\kappa_x\alpha_m^2-\beta_n^2$, $p_i=-\kappa_z\lambda_i^2-\kappa_x\alpha_m^2-\beta_n^2$, ϕ_n and X_n equal $\phi_{m,n}$ and $X_{m,n}$ with $\alpha_m=0$, respectively, and the eigenvalues λ_0 and λ_i are, respectively, the roots of the following equations:

$$e^{2\lambda_0}=\frac{-\gamma\,\kappa_z\,\lambda_0^2+\kappa_z\,\lambda_0+\gamma\,(\kappa_x\,\alpha_m^2+\beta_n^2)}{\gamma\,\kappa_z\,\lambda_0^2+\kappa_z\,\lambda_0-\gamma\,(\kappa_x\,\alpha_m^2+\beta_n^2)} \tag{40}$$

$$\tan\lambda_i=\frac{-\gamma(\kappa_z\,\lambda_i^2+\kappa_x\,\alpha_m^2+\beta_n^2)}{\kappa_z\,\lambda_i} \tag{41}$$

The determination for those eigenvalues is introduced in the next section. Notice that the solution consists of simple series expanded in β_n, double series expanded in β_n and λ_i (or α_m and β_n), and triple series expanded in α_m, β_n and λ_i.

2.3 Evaluations for β_n, λ_0 and λ_i

Application of Newton's method with proper initial guesses to determine the eigenvalues β_n, λ_0 and λ_i has been proposed by Huang et al. (2014) and is briefly introduced herein. The

eigenvalues are situated at the intersection points of the left-hand side (LHS) and RHS functions of Eq. (19) for β_n, Eq. (40) for λ_0, and Eq. (41) for λ_i. Hence, the initial guesses for β_n are considered as $\beta_v - \delta$ if $\beta_v > (\kappa_1\,\kappa_2)^{0.5}$ and as $\beta_v + \delta$ if $\beta_v < (\kappa_1\,\kappa_2)^{0.5}$ where $\beta_v = (2n-1)\pi/(2\,\bar{w}_y)$ and δ is a chosen small value such as 10^{-8} for avoiding being right at the vertical asymptote. In addition, the guess for λ_0 can be formulated as

$$\lambda_{0\,initial} = \delta + \left\{-\kappa_z - \sqrt{\kappa_z[\kappa_z + 4\,\gamma^2(\kappa_x\alpha_m^2 + \beta_n^2)]}\right\}/(2\gamma\kappa_z) \quad (42)$$

where the RHS second term represents the location of the vertical asymptote derived by letting the denominator of the RHS function in Eq. (40) to be zero and solving λ_0 in the resultant equation. Moreover, the guessed value for λ_i is $(2\,i-1)\pi/2 + \delta$.

2.4 Head solution for radial collector well

The lateral of RCW is approximately represented by a line sink composed of a series of adjoining point sinks. The locations of these point sinks are expressed in terms of ($\bar{x}_0 + \bar{l}\cos\theta$, $\bar{y}_0 + \bar{l}\sin\theta$, $\bar{z}_0$) where ($\bar{x}_0$, $\bar{y}_0$, $\bar{z}_0$) = (x_0/y_0, 1, z_0/H) is the central of the lateral, and $\bar{l}$ is a variable to define different locations of the point sink. The solution of head $\bar{h}_w(\bar{x},\bar{y},\bar{z},\bar{t})$ for a lateral can therefore be derived by substituting $\bar{x}_0' = \bar{x}_0 + \bar{l}\cos\theta$, $\bar{y}_0' = 1 + \bar{l}\sin\theta$ and $\bar{z}_0' = \bar{z}_0$ into the point-sink solution, Eq. (30), then by integrating the resultant solution to $\bar{l}$, and finally by dividing the integration result into the sum of lateral lengths. The derivation can be denoted as

$$\bar{h}_w(\bar{x},\bar{y},\bar{z},\bar{t}) = \left(\sum_{k=1}^{N}\bar{L}_k\right)^{-1}\sum_{k=1}^{N}\int_0^{\bar{L}_k}\bar{h}(\bar{x},\bar{y},\bar{z},\bar{t})\,d\bar{l} \quad (43)$$

where $\bar{L}_k = L_k/y_0$ is the *k*-th dimensionless lateral length. Note that the integration variable $\bar{l}$ (i.e., $\bar{x}_0'$ and $\bar{y}_0'$) appears only in X_n and $X_{m,n}$ in Eq. (31). The integral in Eq. (43) can thus be done analytically by integrating X_n and $X_{m,n}$ with respect to $\bar{l}$. After the integration, Eq. (43) can be expressed as

$$\bar{h}_w(\bar{x},\bar{y},\bar{z},\bar{t}) = \left(\sum_{k=1}^{N}\bar{L}_k\right)^{-1}\sum_{k=1}^{N}\begin{cases}\Phi(-\bar{z}_0,\bar{z},1) & \text{for } -\bar{z}_0\le\bar{z}\le 0\\ \Phi(\bar{z},\bar{z}_0,-1) & \text{for } -1\le\bar{z}\le-\bar{z}_0\end{cases} \quad (44)$$

where Φ is defined by Eqs. (31) – (38), and X_n and $X_{m,n}$ in Eq. (31) are replaced, respectively, by

$$X_{n,k} = -G_k/(\beta_n \sin\theta_k) \quad (45)$$

and

$$X_{m,n,k} = \frac{\alpha_m F_k \cos\theta_k + \beta_n G_k \sin\theta_k}{\alpha_m^2 \cos^2\theta_k - \beta_n^2 \sin^2\theta_k} \quad (46)$$

with

$$F_k = \sin(X\alpha_m)[\beta_n \cos(Y\beta_n) + \kappa_1 \sin(Y\beta_n)] - \sin(\bar{x}_0\alpha_m)(\beta_n \cos\beta_n + \kappa_1 \sin\beta_n) \quad (47)$$

$$G_k = \cos(X\alpha_m)[\kappa_1 \cos(Y\beta_n) - \beta_n \sin(Y\beta_n)] - \cos(\bar{x}_0\alpha_m)(\kappa_1 \cos\beta_n - \beta_n \sin\beta_n) \quad (48)$$

where $X = \bar{x}_0 + \bar{L}_k \cos\theta_k$ and $Y = 1 + \bar{L}_k \sin\theta_k$. Notice that Eq. (45) is obtained by substituting $\alpha_m = 0$ into Eq. (46). When $\theta_k = 0$ or π, Eq. (45) reduces to Eq. (49) by applying L'Hospital's rule.

$$X_{n,k} = \bar{L}_k(\beta_n \cos\beta_n + \kappa_1 \sin\beta_n) \quad (49)$$

2.5 SDR solution for radial collector well

On the basis of Darcy's law and the head solution for a RCW, the SDR from streams 1 and 2 can be defined, respectively, as

$$SDR_1(\bar{t}) = -\int_{\bar{x}=0}^{\bar{x}=\bar{w}_x}\left(\int_{\bar{z}=-\bar{z}_0}^{\bar{z}=0}\frac{\partial \bar{h}_w}{\partial \bar{y}}d\bar{z} + \int_{\bar{z}=-1}^{\bar{z}=-\bar{z}_0}\frac{\partial \bar{h}_w}{\partial \bar{y}}d\bar{z}\right)d\bar{x} \quad \text{at} \quad \bar{y} = 0 \quad (50)$$

and

$$SDR_2(\bar{t}) = \int_{\bar{x}=0}^{\bar{x}=\bar{w}_x}\left(\int_{\bar{z}=-\bar{z}_0}^{\bar{z}=0}\frac{\partial \bar{h}_w}{\partial \bar{y}}d\bar{z} + \int_{\bar{z}=-1}^{\bar{z}=-\bar{z}_0}\frac{\partial \bar{h}_w}{\partial \bar{y}}d\bar{z}\right)d\bar{x} \quad \text{at} \quad \bar{y} = \bar{w}_y \quad (51)$$

Again, the double integrals in both equations can be done analytically. Notice that the series term of $2\sum_{m=1}^{\infty}\phi_{m,n}X_{m,n}\cos(\alpha_m \bar{x})$ in Eq. (31) disappears due to the consideration of Eqs. (3) and (4) and the integration with respect to $\bar{x}$ in Eqs. (50) and (51) when deriving the SDR solution. The SDR_1 and SDR_2 are therefore expressed in terms of double series and given below:

$$SDR_1(\bar{t}) = -\frac{2}{\sum_{k=1}^{N}\bar{L}_k}\sum_{k=1}^{N}\sum_{n=1}^{\infty}\left(\psi'_n + \psi'_{n,0} + \sum_{i=1}^{\infty}\psi'_{n,i}\right)X_{n,k}\,Y'_n(0) \quad (52)$$

and

$$SDR_2(\bar{t}) = \frac{2}{\sum_{k=1}^{N} \bar{L}_k} \sum_{k=1}^{N} \sum_{n=1}^{\infty} \left(\psi'_n + \psi'_{n,0} + \sum_{i=1}^{\infty} \psi'_{n,i}\right) X_{n,k}\, Y'_n(\bar{w}_y) \quad (53)$$

with

$$Y'_n(\bar{y}) = \frac{\kappa_1 \beta_n \cos(\beta_n \bar{y}) - \beta_n^2 \sin(\beta_n \bar{y})}{(\beta_n^2 + \kappa_1^2)[\bar{w}_y + \kappa_2 / (\beta_n^2 + \kappa_2^2)] + \kappa_1} \quad (54)$$

$$\psi'_n = -\{\sinh(\bar{z}_0 \lambda'_s) \cosh[(1 - \bar{z}_0)\lambda'_s] + \sinh[(1 - \bar{z}_0)\lambda'_s] \cosh(\bar{z}_0 \lambda'_s)\} / (\kappa_z \lambda'^2_s \sinh \lambda'_s) \quad (55)$$

$$\psi'_{n,0} = -\mu_{n,0}(\theta_{n,0} + \vartheta_{n,0}) / \lambda_0 \quad (56)$$

$$\theta_{n,0} = \cosh[(1 - \bar{z}_0)\lambda_0] \{p'_0 \gamma[-1 + \cosh(\bar{z}_0 \lambda_0) + \kappa_z \lambda_0 \sinh(\bar{z}_0 \lambda_0)]\} \quad (57)$$

$$\vartheta_{n,0} = \sinh[(1 - \bar{z}_0)\lambda_0] [\kappa_z \lambda_0 \cosh(\bar{z}_0 \lambda_0) + p'_0 \gamma \sinh(\bar{z}_0 \lambda_0)] \quad (58)$$

$$\psi'_{n,i} = \nu_{n,i}(\sigma_{n,i} - \eta_{n,i}) / \lambda_i \quad (59)$$

$$\sigma_{n,i} = \cos[(1 - \bar{z}_0)\lambda_i] \{p'_i \gamma[-1 + \cos(\bar{z}_0 \lambda_i)] - \kappa_z \lambda_i \sin(\bar{z}_0 \lambda_i)\} \quad (60)$$

$$\eta_{n,i} = \sin[(1 - \bar{z}_0)\lambda_i] [\kappa_z \lambda_i \cos(\bar{z}_0 \lambda_i) + p'_i \gamma \sin(\bar{z}_0 \lambda_i)] \quad (61)$$

where $\lambda'_s = \beta_n / \sqrt{\kappa_z}$; $p'_0 = \kappa_z \lambda_0^2 - \beta_n^2$; $p'_i = -\kappa_z \lambda_i^2 - \beta_n^2$; $\mu_{n,0}$ equals $\mu_{m,n,0}$ in Eq. (36) with $\alpha_m = 0$; $\nu_{n,i}$ equals $\nu_{m,n,i}$ in Eq. (37) with $\alpha_m = 0$; $X_{n,k}$ is defined in Eq. (45) for $\theta_k \neq 0$ or π and Eq. (49) for $\theta_k = 0$ or π; and λ_0 and λ_i are the roots of Eqs. (40) and (41) with $\alpha_m = 0$, respectively.

2.6 Special cases of the present solution

2.6.1 Confined aquifer of finite extent

If γ = 0 (i.e., S_y = 0 in Eq. (8)), the top boundary is regarded as an impermeable stratum. The aquifer is then a confined system. Under this circumstance, Eq. (40) reduces to $e^{2\lambda_0} = 1$ having the root of $\lambda_0 = 0$, and Eq. (41) yields $\tan \lambda_i = 0$ having the roots of $\lambda_i = i\,\pi$ where $i \in 1, 2, 3, \ldots \infty$. With $\gamma = 0$, $\lambda_0 = 0$ and $\lambda_i = i\,\pi$, the head solution for a confined aquifer can be expressed as Eq. (44) with Eqs. (31) – (38) and (45) – (49) where $\psi_{m,n,0}$ in Eq. (32)

371 is replaced by

372 $$\psi_{m,n,0} = -\exp(p_0\,\bar{t})/p_0 \quad (62)$$

373 Similarly, the SDR solution for a confined aquifer can be written as Eqs. (52) and (53) where
374 the RHS function in Eq. (56) reduces to that in Eq. (62) by applying L'Hospital's rule with $\gamma =$
375 0 and $\lambda_0 = 0$.

376 **2.6.2 Confined aquifer of infinite extent**

377 The head solution introduced in section 2.6.1 is applicable to spatiotemporal head
378 distributions in confined aquifers of infinite extent before the lateral boundary effect comes.
379 Wang and Yeh (2008) indicated that the time can be quantified, in our notation, as $t = R^2S_s/(16K_y)$
380 (i.e., $\bar{t} = R^2/(16y_0^2)$ for dimensionless time) where R is the shortest distance between a RCW
381 and aquifer lateral boundary. Prior to the time, the present head solution with N = 1 for a
382 horizontal well in a confined aquifer gives very close results given in Zhan et al. (2001).

383 **2.6.3 Unconfined aquifer of infinite extent**

384 Prior to the beginning time mentioned in section 2.6.2, the absolute value calculated by
385 the present head solution, Eqs. (44) with N = 1, represents drawdown induced by a horizontal
386 well in unconfined aquifers of infinite extent. The calculated drawdown should be close to that
387 from Zhan and Zlotnik (2002) solution for the case of the instantaneous drainage from water
388 table decline.

389 **2.6.4 Unconfined aquifer of semi-infinite extent**

390 When $\kappa_1 \to \infty$ (i.e., $b_1 = 0$), Eq. (14) reduces to the Dirichlet condition of $\bar{h} = 0$ for stream
391 1 in the absence from a low-permeability streambed, and Eq. (19) becomes $\tan(\beta_n \bar{w}_y) =$
392 $-\beta_n/\kappa_2$. In addition, the boundary effect occurring at the other three sides of the aquifer can
393 be neglected prior to the beginning time. Moreover, when N = 1 and $\theta_1 = 0$, a RCW can be
394 regarded as a horizontal well parallel to stream 1. Under these three conditions, the present
395 head and SDR predictions are close to those in Huang et al. (2011), the head solution of which

agrees well with measured data from a field experiment executed by Mohamed and Rushton (2006). On the other hand, before the time when the boundary effect occurs at $\bar{x} = 0$, $\bar{x} = \bar{w}_x$ and $\bar{y} = \bar{w}_y$, the present head and SDR solutions for a RCW give close predictions to those in Huang et al. (2012), the head and SDR solutions of which agree well with observation data taken from two field experiments carried out by Schafer (2006) and Jasperse (2009), respectively.

2.7 Sensitivity analysis

The hydraulic parameters determined from field observed data are inevitably subject to measurement errors. Consequently, head predictions from the analytical model have uncertainty due to the propagation of measurement errors. Sensitivity analysis can be considered as a tool of exploring the response of the head to the change in a specific parameter (Zheng and Bennett, 2002). One may define the normalized sensitivity coefficient as

$$S_{i,t} = \frac{P_i}{H}\frac{\partial h}{\partial P_i} \tag{63}$$

where $S_{i,t}$ is the normalized sensitivity coefficient for the ith parameter at time t, and P_i represents the magnitude of the ith parameter. Eq. (63) can be approximated as

$$S_{i,t} = \frac{h(P_i + \Delta P_i) - h(P_i)}{\Delta P_i} \times \frac{P_i}{H} \tag{64}$$

where ΔP_i is an increment chosen as $10^{-3}\, P_i$ (Yeh et al., 2008).

3. Results and discussion

This section demonstrates head and SDR predictions and explores some physical insights regarding flow behavior. In section 3.1, groundwater flow and equipotential lines induced by pumping are discussed. In section 3.2, the influence of anisotropy on spatial head and temporal SDR distributions is studied. In section 3.3, the sensitivity analysis is performed to investigate the response of the head to the change in each hydraulic parameter. In section 3.4, the effects of the vertical flow and well depth on temporal SDR distributions for confined and unconfined

aquifers are investigated. For conciseness, we consider a RCW with two laterals with $N = 2$, $\bar{L}_1 = \bar{L}_2 = 0.5$, $\theta_1 = 0$ and $\theta_2 = \pi$. The well can be viewed as a horizontal well parallel to streams 1 and 2. The default values for the other dimensionless parameters are $\bar{w}_x = \bar{w}_y = 2$, $\gamma = 100$, $\bar{x}_0 = 1$, $\bar{y}_0 = 1$, $\bar{z}_0 = 0.5$, $\kappa_x = \kappa_z = 1$, and $\kappa_1 = \kappa_2 = 20$.

3.1 Groundwater flow and hydraulic head

Most existing models assume 2-D flow with neglecting the vertical flow for pumping at a horizontal well (e.g., Mohamed and Rushton, 2006; Haitjema et al., 2010). The head distributions predicted by those models are inaccurate if an observation well is close to the region where the vertical flow prevails. Figure 2 demonstrates the streamlines and equipotential lines predicted by the present solution for a horizontal well in an unconfined aquifer for $\bar{x}_0 = 10$, $\bar{w}_x = \bar{w}_y = 20$ and $\kappa_z = 0.1$, 1, and 10. The well is located at $9.5 \le \bar{x} \le 10.5$, $\bar{y} = 1$ and $\bar{z} = 0.5$ as illustrated in the figure. The equipotential lines are based on steady-state head distributions plotted by Eq. (44) with $\bar{y} = 1$ and $\bar{t} = 10^7$. The stream function ψ can be derived via the Cauchy-Riemann equation, in our notation, as

$$\frac{\partial \bar{\psi}}{\partial \bar{x}} = -\sqrt{\kappa_z}\,\frac{\partial \bar{h}_w}{\partial \bar{z}} \tag{65}$$

where $\bar{\psi} = K_y H \psi / Q$ is the dimensionless stream function describing 2-D streamlines at the vertical plane of $\bar{y} = 1$ based on $\bar{h}_w$ in Eq. (44) with $\bar{t} = 10^7$ for steady state. The function $\bar{\psi}$ is obtained firstly by substituting Eq. (44) into Eq. (65), then by differentiating the result with respect to $\bar{z}$, and eventually by integrating the differentiation result to $\bar{x}$. The coefficient arising from the integration is determined by the condition of $\bar{\psi} = 0$ at $\bar{x} = \bar{x}_0$. The detailed derivation of the stream function is shown in Appendix C. When $\kappa_z = 0.1$, in the range of $10 \le \bar{x} \le 13.66$, the contours of the hydraulic head are in a curved path, and the flow toward the well is slanted. Moreover, the range decreases to $10 \le \bar{x} \le 11.5$ when $\kappa_z = 1$ and to $10 \le \bar{x} \le 10.82$ when $\kappa_z = 10$. Beyond these ranges, the head contours are nearly vertical, and the flow

is essentially horizontal. Define $\bar{d} = d/y_0$ as a shortest dimensionless horizontal distance between the well and a nearest location of only horizontal flow. The $\bar{d}$ is therefore chosen as 3.16, 1 and 0.32 for the cases of κ_z = 0.1, 1 and 10, respectively. Substituting (κ_z, $\bar{d}$) = (0.1, 3.16), (1, 1) and (10, 0.32) into $\kappa_z \bar{d}^2$ leads to about unity. We may therefore conclude that the vertical flow at an observation location is negligible if a shortest dimensionless horizontal distance between the location and a RCW is less than $\bar{d} = \sqrt{1/\kappa_z}$ (i.e., $d = H\sqrt{K_y/K_z}$) for thin aquifers, observation locations far from the well, and/or a small ratio of K_y/K_z.

3.2 Anisotropy analysis of hydraulic head and stream depletion rate

Previous articles have seldom analyzed flow behavior for anisotropic aquifers, i.e., κ_x (K_x/K_y) $\neq$ 1. Head predictions based on the models, developed for isotropic aquifers, will be inaccurate if $\kappa_x \neq 1$. Consider $\bar{w}_x = \bar{w}_y = 2$, $\bar{t} = 10^7$ for steady-state head distributions, and a RCW with $\bar{L}_1 = \bar{L}_2 = 0.25$, $\theta_1 = 0$, $\theta_2 = \pi$, and $(\bar{x}_0, \bar{y}_0, \bar{z}_0)$ = (1, 1, -0.5) for symmetry. The contours of the dimensionless head at $\bar{z} = -0.5$ are shown in Figures 3(a) – 3(d) for κ_x = 1, 10 and 50, 10^{-3}, and 10^{-4}, respectively. The figure indicates that the anisotropy causes a significant effect on the head distributions in comparison with the case of κ_x = 1. In Figure 3(b), the contours exhibit smooth curves in the strip regions of $1 \leq \bar{y} \leq 1.45$ for the case of κ_x = 10 and $1 \leq \bar{y} \leq 1.2$ for the case of κ_x = 50. For the region of $\bar{y} \geq 1.45$, the predicted heads for both cases agree well, and all the contour lines are parallel, indicating that the flow is essentially unidirectional. Substituting (κ_x, $\bar{y}$) = (10, 1.45) and (50, 1.2) into $\kappa_x (\bar{y} - 1)^2$ results in a value about 2. Accordingly, we may draw the conclusion that plots from the inequality of $\kappa_x (\bar{y} - 1)^2 \leq 2$ indicate the strip region for κ_x being greater than 10. Some existing models assuming 2-D flow in a vertical plane with neglecting the flow component along a horizontal well give accurate head predictions beyond the region (e.g., Anderson, 2000; Anderson, 2003; Kompani-Zare et al., 2005).

Aquifers with $K_yH \geq 10^3$ m^2/day can efficiently produce plenty of water from a well. RCWs usually operate with $Q \leq 10^5$ m^3/day for field experiments (e.g., Schafer, 2006; Jasperse, 2009). We therefore define significant dimensionless head drop as $|\bar{h}| > 10^{-5}$ (i.e., $|h| > 1$ mm). The anisotropy of κ_x <1 produces the drop in the strip areas of $1 \leq \bar{x} \leq 1.48$ for the case of $\kappa_x = 10^{-3}$ in Figure 3(c) and $1 \leq \bar{y} \leq 1.32$ for the case of $\kappa_x = 10^{-4}$ in Figure 3(d). Substituting (κ_x, $\bar{x}$) = (10^{-3}, 1.48) and (10^{-4}, 1.32) into $(\bar{x} - \bar{x}_0 - \bar{L}_1)^2/\kappa_x$ approximates 52.9. This result leads to the conclusion that the area can be determined by the inequalities of $(\bar{x} - \bar{x}_0 - \bar{L}_1)^2 \leq 52.9\kappa_x$ and $(\bar{x} - \bar{x}_0 + \bar{L}_2)^2 \leq 52.9\kappa_x$ for any value of κ_x in the range κ_x <1. For a RCW with irregular lateral configurations, the inequalities become $(\bar{x} - \max \bar{x}_k)^2 \leq 52.9\ \kappa_x$ and $(\bar{x} - \min \bar{x}_k)^2 \leq 52.9\kappa_x$ where $\bar{x}_k$ is coordinate $\bar{x}$ of the far end of the k-th lateral. The conclusion applies in principle to reduction in grid points for numerical solutions based on finite difference methods or finite element methods. On the other hand, we have found that Eq. (52) or (53) with various κ_x predicts the same temporal SDR distribution (not shown), indicating that the SDR is independent of κ_x.

3.3 Sensitivity analysis of hydraulic head

Consider an unconfined aquifer of H = 20 m and $w_x = w_y$ = 800 m with a RCW having two laterals of $L_1 = L_2$ = 50 m, θ_1 = 0 and $\theta_2 = \pi$ and two piezometers installed at point A of (400 m, 340 m, −10 m) and point B of (400 m, 80 m, −10 m) illustrated in Figure 4. As discussed in section 3.1, the temporal head distribution at point A exhibits the unconfined behavior in Figure 4(a) because of $\kappa_z\ \bar{d}^2$<1 while at point B displays the confined one in Figure 4(b) due to $\kappa_z\ \bar{d}^2$>1. The sensitivity analysis is conducted with the aid of equation (64) to observe head responses at these two piezometers to the change in each of K_x, K_y, K_z, S_s, S_y, K_1, L_1 and z_0. The temporal distribution curves of the normalized sensitivity coefficients for those eight parameters are shown in Figures 4(a) for point A and 4(b) for point B when $K_x = K_y$ = 1

492 m/day, K_z = 0.1 m/day, S_s = 10^{-5} m^{-1}, S_y = 0.2, K_1 = K_2 = 0.1 m/day, b_1 = b_2 = 1 m, Q = 100
493 m^3/day, x_0 = y_0 = 400 m, and z_0 = 10 m. The figure demonstrates that the hydraulic heads at
494 both piezometers are most sensitive to the change in K_y, second sensitive to the change in K_x
495 and thirdly sensitive to the change in S_y, indicating that K_y, K_x and S_y are the most crucial factors
496 in designing a pumping system. This figure also shows that the heads at point A is sensitive to
497 the change in S_s at the early period of 4×10^{-3} day < t < 10^{-1} day but at point B is insensitive to
498 the change over the entire period. In addition, the head at point A is sensitive to the changes in
499 K_z and z_0 due to 3-D flow (i.e., $\kappa_z \bar{d}^2 < 1$) as discussed in section 3.1. In contrast, the head at
500 point B is insensitive to the changes in K_z and z_0 because the vertical flow diminishes (i.e.,
501 $\kappa_z \bar{d}^2 > 1$). Moreover, the head at point A is sensitive to the change in L_1 but the head at point
502 B is not because its location is far away from the well. Furthermore, the normalized sensitivity
503 coefficient of K_1 for point A away from stream 1 approaches zero but for point B in the vicinity
504 of stream 1 increases with time and finally maintains a certain value at the steady state.
505 Regarding the sensitivity analysis of SDR, Huang et al. (2014) has performed the sensitivity
506 analysis of normalized coefficients of SDR_1 to the changes in K_y, K_1 and S_s for a confined
507 aquifer and in K_y, K_z, K_1, S_s and S_y for an unconfined aquifer.

508 **3.4 Effects of vertical flow and well depth on stream depletion rate**

509 Huang et al. (2014) reveals that the effect of the vertical flow on SDR induced by a vertical
510 well is dominated by the magnitude of the key factor κ_z (i.e., $K_z y_0^2/(K_y H^2)$) where y_0 herein
511 is a distance between stream 1 and the vertical well. They concluded that the effect is negligible
512 when $\kappa_z \geq 10$ for a leaky aquifer. The factor should be replaced by $\kappa_z \bar{a}^2$ (i.e., $K_z a^2/(K_y H^2)$)
513 where a is a shortest distance measured from stream 1 to the end of a lateral of a RCW, and
514 $\bar{a} = a/y_0 = 1$ in this study due to N = 2, θ_1 = 0 and θ_2 = π. We investigate SDR in response to
515 various $\bar{z}_0$ and $\kappa_z \bar{a}$ for unconfined and confined aquifers. The temporal SDR_1 distributions
516 predicted by Eq. (52) for stream 1 adjacent to an unconfined aquifer are shown in Fig. 5(a) for

517 $\bar{z}_0$ = 0.5 and $\kappa_z\bar{a}^2$ = 0.01, 0.1, 1, 10, 20 and 30 and Fig. 5(b) for $\kappa_z\bar{a}^2$ = 1 and 30 when $\bar{z}_0$ =
518 0.1, 0.3, 0.5, 0.7 and 0.9. The curves of SDR_1 versus $\bar{t}$ is plotted in both panels by the present
519 SDR solution for a confined aquifer. In Fig. 5(a), the present solution for an unconfined aquifer
520 predicts a close SDR_1 to that for the confined aquifer when $\kappa_z\bar{a}^2$ = 0.01, indicating that the
521 vertical flow in the unconfined aquifer is ignorable. The SDR_1 for the unconfined aquifer with
522 $\kappa_z\bar{a}^2$ = 30 behaves like that for a confined one, indicating the vertical flow is also ignorable.
523 The SDR_1 is therefore independent of well depths $\bar{z}_0$ when $\kappa_z\bar{a}^2$ = 30 as shown in Fig. 5(b).
524 We may therefore conclude that, under the condition of $\kappa_z\bar{a}^2 \leq 0.01$ or $\kappa_z\bar{a}^2 \geq 30$, a 2-D
525 horizontal flow model can give good predictions in SDR_1 for unconfined aquifers. In contrast,
526 SDR_1 increases with decreasing $\kappa_z\bar{a}^2$ when $0.01 < \kappa_z\bar{a}^2 < 30$ in Fig. 5(a), indicating that the
527 vertical flow component induced by pumping in unconfined aquifers significantly affects SDR_1.
528 The effect of well depth $\bar{z}_0$ on SDR_1 is also significant as shown in Fig. 5(b) when $\kappa_z\bar{a}^2$ = 1.
529 Obviously, the vertical flow effect should be considered in a model when $0.01 < \kappa_z\bar{a}^2 < 30$
530 for unconfined aquifers.

531 It is interesting to note that the SDR_1 or SDR_2 induced by two laterals (i.e., $\theta_1 = 0$ and θ_2
532 $= \pi$) parallel to the streams adjacent to a confined aquifer is independent of $\kappa_z\bar{a}^2$ and $\bar{z}_0$ but
533 depends on aquifer width of $\bar{w}_y$. The temporal SDR distribution curves based on Eqs. (52) and
534 (53) with γ = 0 for a confined aquifer with $\bar{w}_y$ = 2, 4, 6, 10 and 20 are plotted in Fig. 6. The
535 dimensionless distance between the well and stream 1 is set to unity (i.e., $\bar{y}_0 = 1$) for each
536 case. The SDR_1 predicted by Hunt (1999) solution based on a vertical well in a confined aquifer
537 extending infinitely is considered. The present solution for each $\bar{w}_y$ gives the same SDR_1 as
538 the Hunt solution before the time when stream 2 contributes filtration water to the aquifer and
539 influences the supply of SDR_1. It is interesting to note that the sum of steady-state SDR_1 and
540 SDR_2 is always unity for a fixed $\bar{w}_y$. The former and latter can be estimated by $(\bar{w}_y - 1)/\bar{w}_y$

and $1/\bar{w}_y$, respectively. Such a result corresponds with that in Sun and Zhan (2007) which investigates the distribution of steady-state SDR_1 and SDR_2 induced by a vertical well.

4. Concluding remarks

This study develops a new analytical model describing 3-D flow induced by a RCW in a rectangular confined or unconfined aquifer bounded by two parallel streams and no-flow stratums in the other two sides. The flow equation in terms of the hydraulic head with a point sink term is employed. Both streams fully penetrate the aquifer and are under the Robin condition in the presence of low-permeability streambeds. A first-order free surface equation (8) describing the water table decline gives good predictions when the conditions $|h|/H \leq 0.1$ and $|\partial h/\partial x| + |\partial h/\partial y| \leq 0.01$ are satisfied. The flux across the well screen might be uniform on a lateral within 150 m. The head solution for the point sink is expressed in terms of a triple series derived by the methods of Laplace transform and finite integral transform. The head solution for a RCW is then obtained by integrating the point-sink solution along the laterals and dividing the integration result by the sum of lateral lengths. The integration can be done analytically due to the aquifer of finite extent with Eqs. (3) − (6). On the basis of Darcy's law and the head solution, the SDR solution for two streams can also be acquired. The double integrals of defining the SDR in Eqs. (50) and (51) can also be done analytically due to considerations of Eqs. (3) − (6). The sensitivity analysis is performed to explore the response of the head to the change in each of the hydraulic parameters and variables. New findings regarding the responses of flow and SDR to pumping at a RCW are summarized below:

1. Groundwater flow in a region based on $\bar{d} = \sqrt{1/\kappa_z}$ is 3-D, and temporal head distributions exhibit the unconfined behavior. A mathematical model should consider 3-D flow when predicting the hydraulic head in the region. Beyond this region, groundwater flow is horizontal, and temporal head distributions display the confined behavior. A 2-D flow model can predict accurate hydraulic head.

2. The aquifer anisotropy of κ_x >10 causes unidirectional flow in the strip region determined based on $\kappa_x\,(\bar{y}-1)^2 > 2$ for a horizontal well. Existing models assuming 2-D flow in a vertical plane with neglecting the flow component along the well give accurate head predictions in the region.
3. The aquifer anisotropy of κ_x <1 produces significant change in the head (i.e., $|\bar{h}| > 10^{-5}$ or $|h| > 1$ mm) in the strip area determined by $(\bar{x}-\max\bar{x}_k)^2 \le 52.9\,\kappa_x$ and $(\bar{x}-\min\bar{x}_k)^2 \le 52.9\kappa_x$ for a RCW with irregular lateral configurations.
4. The hydraulic head in the whole domain is most sensitive to the change in K_y, second sensitive to the change in K_x, and thirdly sensitive to the change in S_y. They are thus the most crucial factors in designing a pumping system.
5. The hydraulic head is sensitive to changes in K_z, S_s, z_0 and L_k in the region of $\bar{d} < \sqrt{1/\kappa_z}$ and is insensitive to the changes of them beyond the region.
6. The hydraulic head at observation locations near stream 1 is sensitive to the change in K_1 but away from the stream isn't.
7. The effect of the vertical flow on SDR is ignorable when $\kappa_z\bar{a}^2 \le 0.01$ or $\kappa_z\bar{a}^2 \ge 30$ for unconfined aquifers. In contrast, neglecting the effect will underestimate SDR when $0.01 < \kappa_z\bar{a}^2 < 30$.
8. For unconfined aquifers, SDR increases with dimensionless well depth $\bar{z}_0$ when $0.01 < \kappa_z < 30$ and is independent of $\bar{z}_0$ when $\kappa_z \le 0.01$ or $\kappa_z \ge 30$. For confined aquifers, SDR is independent of $\bar{z}_0$ and κ_z. For both kinds of aquifers, the distribution curve of SDR versus $\bar{t}$ is independent of aquifer anisotropy κ_x.

Acknowledgements.

Research leading to this paper has been partially supported by the grants from the Taiwan

590 Ministry of Science and Technology under the contract NSC 102 – 2221 – E – 009 – 072 –
591 MY2, MOST 103 – 2221 – E – 009 – 156, and MOST 104 – 2221 – E – 009 – 148 – MY2.
592

593 **Appendix A: Finite integral transform**

594 Latinopoulos (1985) provided the finite integral transform for a rectangular aquifer
595 domain where each side can be under either the Dirichlet, no-flow, or Robin condition. The
596 transform associated with the boundary conditions, Eqs. (12) – (15), is defined as

597 $$\tilde{h}(\alpha_m,\beta_n)=\Im\{\bar{h}(\bar{x},\bar{y})\}=\int_0^{\bar{w}_x}\int_0^{\bar{w}_y}\bar{h}(\bar{x},\bar{y})\ \cos(\alpha_m\,\bar{x})\,K(\bar{y})\,d\bar{y}\,d\bar{x} \quad \text{(A1)}$$

598 with

599 $$K(\bar{y})=\sqrt{2}\,\frac{\beta_n\cos(\beta_n\,\bar{y})+\kappa_1\sin(\beta_n\,\bar{y})}{\sqrt{(\beta_n^2+\kappa_1^2)[\bar{w}_y+\kappa_2/(\beta_n^2+\kappa_2^2)]+\kappa_1}} \quad \text{(A2)}$$

600 where $\cos(\alpha_m\,\bar{x})\ K(\bar{y})$ is the kernel function. According to Latinopoulos (1985, Eq. (9)), the
601 transform has the property of

602 $$\Im\left\{\kappa_x\frac{\partial^2\bar{h}}{\partial\bar{x}^2}+\frac{\partial^2\bar{h}}{\partial\bar{y}^2}\right\}=-(\kappa_x\,\alpha_m^2+\beta_n^2)\,\tilde{h}(\alpha_m,\beta_n) \quad \text{(A3)}$$

603 The formula for the inverse finite integral transform can be written as (Latinopoulos, 1985, Eq.
604 (14))

605 $$\bar{h}(\bar{x},\bar{y})=\Im^{-1}\left\{\tilde{h}(\alpha_m,\beta_n)\right\}=\frac{1}{\bar{w}_x}\left[\sum_{n=1}^{\infty}\tilde{h}(0,\beta_n)K(\bar{y})+2\sum_{m=1}^{\infty}\sum_{n=1}^{\infty}\tilde{h}(\alpha_m,\beta_n)\cos(\alpha_m\,\bar{x})K(\bar{y})\right] \quad \text{(A4)}$$

606

607 **Appendix B: Derivation of equation (31)**

608 The function of p in Eq. (28) is defined as

609 $$F(p)=\frac{\cosh[(1+a)\lambda][-\kappa_z\lambda\cosh(b\lambda)+cp\gamma\sinh(b\lambda)]}{p\,\kappa_z\lambda(p\gamma\cosh\lambda+\kappa_z\lambda\sinh\lambda)} \quad \text{(B1)}$$

610 Notice that the term $\cos(\alpha_m\bar{x}_0)K(\bar{y}_0)$ in Eq. (28) is excluded because it is independent of p.
611 $F(p)$ is a single-value function with respect to p. On the basis of the residue theorem, the

inverse Laplace transform for $F(p)$ equals the summation of residues of poles in the complex plane. The residue of a simple pole can be derived according to the formula below:

$$\text{Res}|_{p=p_i} = \lim_{p \to p_i} F(p) \exp(p\bar{t}) \, (p - p_i) \tag{B2}$$

where p_i is the location of the pole in the complex plane.

The locations of poles are the roots of the equation obtained by letting the denominator in Eq. (B1) to be zero, denoted as

$$p \, \kappa_z \, \lambda (p \, \gamma \cosh \lambda + \kappa_z \, \lambda \sinh \lambda) = 0 \tag{B3}$$

where λ is defined in Eq. (29). Notice that $p = -\kappa_x \alpha_m^2 - \beta_n^2$ obtained by $\lambda = 0$ is not a pole in spite of being a root. Apparently, one pole is at $p = 0$, and the residue based on Eq. (B2) with $p_i = 0$ is expressed as

$$\text{Res}|_{p=0} = \lim_{p \to 0} \frac{\cosh[(1+a)\lambda][-\kappa_z \lambda \cosh(b\lambda) + cp\gamma \sinh(b\lambda)]}{\kappa_z \lambda (p\gamma \cosh \lambda + \kappa_z \lambda \sinh \lambda)} \exp(p\bar{t}) \tag{B4}$$

Eq. (B4) with $p = 0$ and $\lambda = \lambda_s$ reduces to $\psi_{m,n}$ in Eq. (33).

Other poles are determined by the equation of

$$p \, \gamma \cosh \lambda + \kappa_z \, \lambda \sinh \lambda = 0 \tag{B5}$$

which comes from Eq. (B3). One pole is at $p = p_0$ between $p = 0$ and $p = -\kappa_x \, \alpha_m^2 - \beta_n^2$ in the negative part of the real axis. Newton's method can be used to obtain the value of p_0. In order to have proper initial guess for Newton's method, we let $\lambda = \lambda_0$ and then have $p = \kappa_z \, \lambda_0^2 - \kappa_x \, \alpha_m^2 - \beta_n^2$ based on Eq. (29). Substituting $\lambda = \lambda_0$, $p = \kappa_z \, \lambda_0^2 - \kappa_x \, \alpha_m^2 - \beta_n^2$, $\cosh \lambda_0 = (e^{\lambda_0} + e^{-\lambda_0})/2$ and $\sinh \lambda_0 = (e^{\lambda_0} - e^{-\lambda_0})/2$ into Eq. (B5) and rearranging the result leads to Eq. (40). Initial guess for finding root λ_0 of Eq. (40) is discussed in section 2.3. With known value of λ_0, one can obtain $p_0 = \kappa_z \, \lambda_0^2 - \kappa_x \, \alpha_m^2 - \beta_n^2$. According to Eq. (B2), the residue of the simple pole at $p = p_0$ is written as

$$\text{Res}|_{p=p_0} = \lim_{p \to p_0} \frac{\cosh[(1+a)\lambda][-\kappa_z \lambda \cosh(b\lambda) + cp\gamma \sinh(b\lambda)]}{p\kappa_z \lambda (p\gamma \cosh \lambda + \kappa_z \lambda \sinh \lambda)} \exp(p\bar{t}) \, (p - p_0) \tag{B6}$$

where both the denominator and nominator equal zero when $p = p_0$. Applying L'Hospital's

Rule to Eq. (B6) results in

$$\mathrm{Res}|_{p=p_0} = \lim_{p\to p_0} \frac{2\cosh[(1+a)\lambda][-\kappa_z\lambda\cosh(b\lambda)+cp\gamma\sinh(b\lambda)]}{p[(1+2\gamma)\kappa_z\lambda\cosh\lambda+(\gamma p+\kappa_z)\sinh\lambda]}\exp(p\bar{t}) \quad \text{(B7)}$$

Eq. (B7) with $p = p_0$ and $\lambda = \lambda_0$ reduces to $\psi_{m,n,0}$ in Eq. (34).

On the other hand, infinite poles are at $p = p_i$ behind $p = -\kappa_x\,\alpha_m^2 - \beta_n^2$. Similar to the derivation of Eq. (40), we let $\lambda = \sqrt{-1}\lambda_i$ and then have $p = -\kappa_z\,\lambda_i^2 - \kappa_x\,\alpha_m^2 - \beta_n^2$ based on Eq. (29). Substituting $\lambda = \sqrt{-1}\lambda_i$, $p = -\kappa_z\,\lambda_i^2 - \kappa_x\,\alpha_m^2 - \beta_n^2$, $\cosh\lambda = \cos\lambda_i$ and $\sinh\lambda = \sqrt{-1}\sin\lambda_i$ into Eq. (B3) and rearranging the result yields Eq. (41). The determination of λ_i is discussed in section 2.3. With known value λ_i, one can have $p_i = -\kappa_z\,\lambda_i^2 - \kappa_x\,\alpha_m^2 - \beta_n^2$. The residues of those simple poles at $p=p_i$ can be expressed as $\psi_{m,n,i}$ in Eq. (35) by substituting $p_0 = p_i$, $p = p_i$, $\lambda = \sqrt{-1}\lambda_i$, $\cosh\lambda = \cos\lambda_i$ and $\sinh\lambda = \sqrt{-1}\sin\lambda_i$ into Eq. (B7). Eventually, the inverse Laplace transform for $F(p)$ equals the sum of those residues (i.e., $\phi_{m,n} = \psi_{m,n} + \psi_{m,n,0} + \sum_{i=1}^{\infty}\psi_{m,n,i}$). The time-domain result of $\Omega(a,b,c)$ in Eq. (28) is then obtained as $\phi_{m,n}\cos(\alpha_m\bar{x}_0)K(\bar{y}_0)$. By substituting $\tilde{h}(\alpha_m,\beta_n) = \phi_{m,n}\cos(\alpha_m\bar{x}_0)K(\bar{y}_0)$ and $\tilde{h}(0,\beta_n) = \phi_n K(\bar{y}_0)$ into Eq. (A4) and letting $\bar{h}(\bar{x},\bar{y})$ to be $\Phi(a,b,c)$, the inverse finite integral transform for the result can be derived as

$$\Phi(a,b,c) = \frac{1}{\bar{w}_x}\Big[\sum_{n=1}^{\infty}\big(\phi_n\,K(\bar{y}_0)K(\bar{y}) + 2\sum_{m=1}^{\infty}\phi_{m,n}\cos(\alpha_m\bar{x}_0)K(\bar{y}_0)\cos(\alpha_m\,\bar{x})\,K(\bar{y})\big)\Big] \quad \text{(B8)}$$

Moreover, Eq. (B8) reduces to Eq. (31) when letting the terms of $K(\bar{y}_0)K(\bar{y})$ and $\cos(\alpha_m\bar{x}_0)K(\bar{y}_0)\,K(\bar{y})$ to be $2X_nY_n$ and $2X_{m,n}Y_n$, respectively.

Appendix C: Derivation of $\bar{\psi}$ in Eq. (65)

The dimensionless stream function $\bar{\psi}$ in Eq. (65) can be expressed as

$$\bar{\psi} = C - \sqrt{\kappa_z}\int \partial\bar{h}_w/\partial\bar{z}\,d\bar{x} \text{ at } \bar{y} = 1 \text{ and } \bar{t} = 10^7 \quad \text{(C1)}$$

where C is a coefficient resulting from the integration, and $\bar{h}_w$ is defined in Eq. (44).

Substituting Eq. (44) into Eq. (C1) leads to

$$\overline{\psi}(\bar{x},\bar{z}) = C - \frac{\sqrt{\kappa_z}}{\sum_{k=1}^{N}\bar{L}_k}\sum_{k=1}^{N}\begin{cases}\int \partial\Phi(-\bar{z}_0,\bar{z},1)/\partial\bar{z}\, d\bar{x} & \text{for } -\bar{z}_0\le\bar{z}\le 0\\ \int \partial\Phi(\bar{z},\bar{z}_0,-1)/\partial\bar{z}\, d\bar{x} & \text{for } -1\le\bar{z}\le-\bar{z}_0\end{cases} \text{ at } \bar{y}=1 \text{ and } \bar{t}=10^7 \quad \text{(C2)}$$

$$\Phi(a,b,c) = \frac{2}{\bar{w}_x}\left\{\sum_{n=1}^{\infty}\left[\phi_n\, X_{n,k} + 2\sum_{m=1}^{\infty}\phi_{m,n}\, X_{m,n,k}\, \cos(\alpha_m\,\bar{x})\right] Y_n\right\} \quad \text{(C3)}$$

where $\phi_{m,n}, Y_n, X_{n,k}$ and $X_{m,n,k}$ are defined in Eqs. (32), (38), (45) and (46), respectively, and ϕ_n equals $\phi_{m,n}$ with $\alpha_m = 0$. In Eq. (C3), variable $\bar{x}$ appears only in $\cos(\alpha_m\,\bar{x})$, and variable $\bar{z}$ appears only in ϕ_n and $\phi_{m,n}$ in Eq. (32). Eq. (C2) therefore becomes

$$\overline{\psi}(\bar{x},\bar{z}) = C - \frac{\sqrt{\kappa_z}}{\sum_{k=1}^{N}\bar{L}_k}\sum_{k=1}^{N}\begin{cases}\Phi'(-\bar{z}_0,\bar{z},1) & \text{for } -\bar{z}_0\le\bar{z}\le 0\\ \Phi'(-\bar{z}_0,\bar{z},1) & \text{for } -1\le\bar{z}\le-\bar{z}_0\end{cases} \text{ at } \bar{y}=1 \text{ and } \bar{t}=10^7 \quad \text{(C4)}$$

$$\Phi'(a,b,c) = \frac{2}{\bar{w}_x}\left\{\sum_{n=1}^{\infty}\left[\frac{\partial\phi_n}{\partial\bar{z}}\, X_{n,k}\int d\bar{x} + 2\sum_{m=1}^{\infty}\frac{\partial\phi_{m,n}}{\partial\bar{z}}\, X_{m,n,k}\int \cos(\alpha_m\,\bar{x})\, d\bar{x}\right] Y_n\right\} \quad \text{(C5)}$$

Consider $\bar{t}=10^7$ for steady-state flow that the exponential terms of $\exp(p_0\,\bar{t})$ and $\exp(p_i\,\bar{t})$ approach zero (i.e., $p_0>0$ and $p_i>0$) for the default values of the parameters used to plot Figure 2. Then, we have $\phi_{m,n}=\psi_{m,n}$ defined in Eq. (33) because of $\psi_{m,n,0}\cong 0$, $\psi_{m,n,i}\cong 0$, $\mu_{m,n,0}\cong 0$ and $\nu_{m,n,i}\cong 0$. On the basis of $\phi_{m,n}=\psi_{m,n}$ and Eq. (33) with $a=-\bar{z}_0$ and $b=\bar{z}$ for $-\bar{z}_0\le\bar{z}\le 0$ and $a=\bar{z}$ and $b=\bar{z}_0$ for $-1\le\bar{z}\le-\bar{z}_0$, the result of differentiation, i.e., $\partial\phi_{m,n}/\partial\bar{z}$, in Eq. (C5) equals

$$\frac{\partial\phi_{m,n}}{\partial\bar{z}} = \begin{cases}-\lambda_s\cosh[(1-\bar{z}_0)\lambda_s]\sinh(\bar{z}\,\lambda_s)/(\kappa_z\,\lambda_s\,\sinh\lambda_s) & \text{for } -\bar{z}_0\le\bar{z}\le 0\\ -\lambda_s\sinh[(1+\bar{z})\lambda_s]\cosh(\bar{z}_0\,\lambda_s)/(\kappa_z\,\lambda_s\,\sinh\lambda_s) & \text{for } -1\le\bar{z}\le-\bar{z}_0\end{cases} \quad \text{(C6)}$$

Notice that $\partial\phi_n/\partial\bar{z}$ in Eq. (C5) equals Eq. (C6) with $\alpha_m=0$. In addition, both integrations in Eq. (C5) can be done analytically as

$$\int \cos(\alpha_m\,\bar{x})\, d\bar{x} = \begin{cases}\sin(\alpha_m\,\bar{x})/\alpha_m & \text{for } \alpha_m\neq 0\\ \bar{x} & \text{for } \alpha_m = 0\end{cases} \quad \text{(C7)}$$

On the other hand, coefficient *C* in Eq. (C4) is determined by the condition of $\overline{\psi}=0$ at $\bar{x}=\bar{x}_0$ and results in

$$C = \frac{\sqrt{\kappa_z}}{\sum_{k=1}^{N}\bar{L}_k}\sum_{k=1}^{N}\begin{cases}\Phi'(-\bar{z}_0,\bar{z},1) & \text{for } -\bar{z}_0\le\bar{z}\le 0\\ \Phi'(-\bar{z}_0,\bar{z},1) & \text{for } -1\le\bar{z}\le-\bar{z}_0\end{cases} \quad \text{(C8)}$$

where Φ' is defined in Eq. (C5) with Eqs. (C6) and (C7), $\bar{x}=\bar{x}_0$ and $\bar{y}=1$.

References

Anderson, E. I.: The method of images for leaky boundaries, Adv. Water Resour., 23, 461–474, doi:10.1016/S0309-1708(99)00044-5, 2000.

Anderson, E. I.: An analytical solution representing groundwater-surface water interaction, Water Resour. Res., 39(3), 1071, doi:10.1029/2002WR001536, 2003.

Anderson, E. I.: Stable pumping rates for horizontal wells in bank filtration systems, Adv. Water Resour., 54, 57–66, doi:10.1016/j.advwatres.2012.12.012, 2013.

Bear, J.: Hydraulics of Groundwater, McGraw-Hill, New York, 84, 1979.

Charbeneau, R. J.: Groundwater Hydraulics and Pollutant Transport, Prentice-Hall, NJ, 57, 2000.

Chen, C. X., Wan, J. W., and Zhan, H. B.: Theoretical and experimental studies of coupled seepage-pipe flow to a horizontal well, J. Hydrol., 281(1–2), 159–171, doi:10.1016/S0022-1694(03)00207-5, 2003.

Chen, X., Dong, W., Ou, G., Wang, Z., and Liu, C.: Gaining and losing stream reaches have opposite hydraulic conductivity distribution patterns, Hydrol. Earth Syst. Sci., 17, 2569–2579, doi:10.5194/hess-17-2569-2013, 2013.

Exner-Kittridge, M., Salinas, J. L., and Zessner, M.: An evaluation of analytical stream to groundwater exchange models: a comparison of gross exchanges based on different spatial flow distribution assumptions, Hydrol. Earth Syst. Sci., 18, 2715–2734, doi:10.5194/hess-18-2715-2014, 2014.

Flipo, N., Mouhri, A., Labarthe, B., Biancamaria, S., Rivière, A., and Weill, P.: Continental hydrosystem modelling: the concept of nested stream–aquifer interfaces, Hydrol. Earth Syst. Sci., 18, 3121–3149, doi:10.5194/hess-18-3121-2014, 2014.

Goldscheider, N., and Drew, D.: Methods in karst hydrology, Taylor & Francis Group, London,

706 UK, 88, 2007.
707 Haitjema, H., Kuzin, S., Kelson, V., and Abrams, D.: Modeling flow into horizontal wells in a
708 Dupuit-Forchheimer model, Ground Water, 48(6), 878−883, doi:10.1111/j.1745-
709 6584.2010.00694.x, 2010.
710 Hantush, M. S. and Papadopoulos, I. S.: Flow of groundwater to collector wells, J. Hydr. Eng.
711 Div., 88(5), 221−244, 1962.
712 Huang, C. S., Chen, Y. L., and Yeh, H. D.: A general analytical solution for flow to a single
713 horizontal well by Fourier and Laplace transforms, Adv. Water Resour., 34(5), 640−648,
714 doi:10.1016/j.advwatres.2011.02.015, 2011.
715 Huang, C. S., Tsou, P. R., and Yeh, H. D.: An analytical solution for a radial collector well
716 near a stream with a low-permeability streambed, J. Hydrol., 446, 48−58,
717 doi:10.1016/j.jhydrol.2012.04.028, 2012.
718 Huang, C. S., Lin, W. S., and Yeh, H. D.: Stream filtration induced by pumping in a confined,
719 unconfined or leaky aquifer bounded by two parallel streams or by a stream and an
720 impervious stratum, J. Hydrol., 513, 28−44, doi:10.1016/j.jhydrol.2014.03.039, 2014.
721 Hunt, B.: Unsteady stream depletion from ground water pumping, Ground Water, 37(1),
722 98−102, doi:10.1111/j.1745-6584.1999.tb00962.x, 1999.
723 Hunt, B.: Flow to vertical and nonvertical wells in leaky aquifers, J. Hydrol. Eng., 10(6),
724 477−484, doi:10.1061/(ASCE)1084-0699(2005)10:6(477), 2005.
725 Jasperse, J.: Planning, design and operations of collector 6, Sonoma County Water Agency,
726 NATO Sci. Peace Secur., 169−202, doi:10.1007/978-94-007-0026-0_11, 2009.
727 Kawecki, M. W.: Transient flow to a horizontal water well, Ground Water, 38(6), 842−850,
728 doi:10.1111/j.1745-6584.2000.tb00682.x, 2000.
729 Kawecki, M. W. and Al-Subaikhy, H. N.: Unconfined linear flow to a horizontal well, Ground
730 Water, 43(4), 606−610, doi:10.1111/j.1745-6584.2005.0059.x, 2005.

Kompani-Zare, M., Zhan, H., and Samani, N.: Analytical study of capture zone of a horizontal well in a confined aquifer, J. Hydrol., 307, 48−59, doi:10.1016/j.jhydrol.2004.09.021, 2005.

Kreyszig, E.: Advanced engineering mathematics, John Wiley & Sons, New York, 258, 1999.

Latinopoulos, P.: Analytical solutions for periodic well recharge in rectangular aquifers with third-kind boundary conditions, J. Hydrol., 77(1), 293−306, 1985.

Lee, E., Hyun, Y., Lee, K. K., and Shin, J.: Hydraulic analysis of a radial collector well for riverbank filtration near Nakdong River, South Korea, Hydrogeol. J., 20(3), 575−589, doi:10.1007/s10040-011-082-3, 2012.

Mohamed, A. and Rushton, K.: Horizontal wells in shallow aquifers: Field experiment and numerical model, J. Hydrol., 329(1−2), 98−109, doi:10.1016/j.jhydrol.2006.02.006, 2006.

Neuman, S. P.: Theory of flow in unconfined aquifers considering delayed response of the water table, Water Resour. Res., 8(4), 1031–1045, 1972.

Nyholm, T., Christensen, S., and Rasmussen, K. R.: Flow depletion in a small stream caused by ground water abstraction from wells, Ground Water, 40(4), 425−437, 2002.

Park, E. and Zhan, H. B.: Hydraulics of a finite-diameter horizontal well with wellbore storage and skin effect, Adv. Water Resour., 25(4), 389−400, doi:10.1016/S0309-1708(02)00011-8, 2002.

Park, E. and Zhan, H. B.: Hydraulics of horizontal wells in fractured shallow aquifer systems, J. Hydrol., 281(1−2), 147−158, doi:10.1016/S0022-1694(03)00206-3, 2003.

Rodriguez, L., Vives, L., and Gomez, A.: Conceptual and numerical modeling approach of the Guarani Aquifer System, Hydrol. Earth Syst. Sci., 17, 295–314, doi:10.5194/hess-17-295-2013, 2013.

Rushton, K. R. and Brassington, F. C.: Significance of hydraulic head gradients within horizontal wells in unconfined aquifers of limited saturated thickness, J. Hydrol., 492,

281−289, doi:10.1016/j.jhydrol.2013.04.006, 2013a.

Rushton, K. R. and Brassington, F. C.: Hydraulic behavior and regional impact of a horizontal well in a shallow aquifer: example from the Sefton Coast, northwest England (UK), Hydrogeol. J., 21(5), 1117−1128, doi:10.1007/s10040-013-0985-0, 2013b.

Schafer, D. C.: Use of aquifer testing and groundwater modeling to evaluate aquifer/river hydraulics at Louisville Water Company, Louisville, Kentucky, USA, NATO Sci. Ser. IV Earth Enviro. Sci., 60, 179−198, doi:10.1007/978-1-4020-3938-6_8, 2006.

Steward, D. R.: Three-dimensional analysis of the capture of contaminated leachate by fully penetrating, partially penetrating, and horizontal wells, Water Resour. Res., 35(2), 461−468, doi:10.1029/1998WR900022, 1999.

Su, G. W., Jasperse, J., Seymour, D., Constantz, J., and Zhou, Q.: Analysis of pumping-induced unsaturated regions beneath a perennial river, Water Resour. Res., 43(8), W08421, doi:10.1029/2006WR005389, 2007.

Sun, D. M. and Zhan, H. B.: Flow to a horizontal well in an aquitard-aquifer system, J. Hydrol., 321(1−4), 364−376, doi:10.1016/j.jhydrol.2005.08.008, 2006.

Sun, D. M. and Zhan, H. B.: Pumping induced depletion from two streams, Adv. Water Resour., 30, 1016−1026, doi:10.1016/j.advwatres.2006.09.001, 2007.

Todd, D. K. and Mays, L. W.: Groundwater hydrology, John Wiley & Sons, Inc., New Jersey, USA, 240, 2005.

Tsou, P. R., Feng, Z. Y., Yeh, H. D., and Huang, C. S.: Stream depletion rate with horizontal or slanted wells in confined aquifers near a stream, Hydrol. Earth Syst. Sc., 14(8), 1477−1485, doi:10.5194/hess-14-1477-2010, 2010.

Unland, N. P., Cartwright, I., Cendón, D. I., and Chisari, R.: Residence times and mixing of water in river banks: implications for recharge and groundwater–surface water exchange, Hydrol. Earth Syst. Sc., 18, 5109−5124, doi:10.5194/hess-18-5109-2014, 2014.

Wang, C. T. and Yeh, H. D.: Obtaining the steady-state drawdown solutions of constant-head and constant-flux tests, Hydrol. Process., 22(17), 3456−3461, doi:10.1002/hyp.6950, 2008.

Yeh, H. D., Chang, Y. C., and Zlotnik, V. A.: Stream depletion rate and volume from groundwater pumping in wedge-shaped aquifers, J. Hydrol., 349(3−4), 501−511, doi:10.1016/j.jhydrol.2007.11.025, 2008.

Yeh, H. D. and Chang, Y. C.: Recent advances in modeling of well hydraulics, Adv. Water Resour., 51, 27−51, doi:10.1016/j.advwatres.2012.03.006, 2013.

Yeh, H. D., Huang, C. S., Chang, Y. C., and Jeng, D. S.: An analytical solution for tidal fluctuations in unconfined aquifers with a vertical beach, Water Resour. Res., 46, W10535, doi:10.1029/2009WR008746, 2010.

Zhan, H. B. and Zlotnik, V. A.: Groundwater flow to a horizontal or slanted well in an unconfined aquifer, Water Resour. Res., 38(7), doi:10.1029/2001WR000401, 2002.

Zhan, H. B. and Park, E.: Horizontal well hydraulics in leaky aquifers, J. Hydrol., 281(1−2), 129−146, doi:10.1016/S0022-1694(03)00205-1, 2003.

Zhan, H. B., Wang, L. V., and Park, E.: On the horizontal-well pumping tests in anisotropic confined aquifers, J. Hydrol., 252(1−4), 37−50, doi:10.1016/S0022-1694(01)00453-X, 2001.

Zheng, C. and Bennett, G. D.: Applied contaminant transport modeling, 2nd ed., Wiley-Interscience, N.Y., 287, 2002.

Zhou, Y., Wenninger, J., Yang, Z., Yin, L., Huang, J., Hou, L., Wang, X., Zhang, D., and Uhlenbrook, S.: Groundwater–surface water interactions, vegetation dependencies and implications for water resources management in the semi-arid Hailiutu River catchment, China – a synthesis, Hydrol. Earth Syst. Sci., 17, 2435–2447, doi:10.5194/hess-17-2435-2013, 2013.

806 Zlotnik, V. A.: A concept of maximum stream depletion rate for leaky aquifers in alluvial
807 valleys, Water Resour. Res., 40(6), W06507, doi:10.1029/2003WR002932, 2004.

808 **Table 1.** Symbols used in the text and their definitions.

Symbol	Definition
a	Shortest horizontal distance between stream 1 and the far end of lateral
$\bar{a}$	a/y_0
b_1, b_2	Thicknesses of streambeds 1 and 2, respectively
d	Shortest horizontal distance between the far end of lateral and location of having only horizontal flow
$\bar{d}$	d/y_0
H	Aquifer thickness
h	Hydraulic head
$\bar{h}$	$(K_y\ H\ h)/Q$
K_x, K_y, K_z	Aquifer hydraulic conductivities in x, y and z directions, respectively
(K_1, K_2)	Hydraulic conductivities of streambeds 1 and 2, respectively
L_k	Length from x axis to k-th lateral where $k \in (1, 2, \ldots N)$
$\bar{L}_k$	L_k/y_0
N	The number of laterals
Q	Pumping rate of point sink or radial collector well
p	Laplace parameter
p_i	$-\kappa_z\lambda_i^2 - \kappa_x\alpha_m^2 - \beta_n^2$
p_i'	$-\kappa_z\ \lambda_i^2 - \beta_n^2$
p_0	$\kappa_z\lambda_0^2 - \kappa_x\alpha_m^2 - \beta_n^2$
p_0'	$\kappa_z\ \lambda_0^2 - \beta_n^2$
R	Shortest horizontal distance between the far end of lateral and aquifer lateral boundary
S_s, S_y	Specific storage and specific yield, respectively
t	Time since pumping
$\bar{t}$	$(K_y\ t)/(S_s\ y_0^2)$
w_x, w_y	Aquifer widths in x and y directions, respectively
$\bar{w}_x$, $\bar{w}_y$	w_x/y_0, w_y/y_0
X_n	Equaling $X_{m,n}$ defined in Eq. (39) with $\alpha_m = 0$
$X_{n,k}$	Defined in Eq. (45)
x, y, z	Cartesian coordinate system
$\bar{x}$, $\bar{y}$, $\bar{z}$	x/y_0, y/y_0, z/H
$\bar{x}_k$	Coordinate $\bar{x}$ of the far end of the k-th lateral

x_0, y_0, z_0	Location of center of RCW
$\bar{x}_0,\ \bar{y}_0,\ \bar{z}_0$	$x_0/y_0,\ 1,\ z_0/H$
$x_0',\ y_0',\ z_0'$	Location of point sink
$\bar{x}_0',\ \bar{y}_0',\ \bar{z}_0'$	$x_0'/y_0,\ y_0'/y_0,\ z_0'/H$
α_m	$m\,\pi/\bar{w}_x$
β_n	Roots of Eq. (19)
ϕ_n	Equaling $\phi_{m,n}$ defined in Eq. (32) with $\alpha_m = 0$
γ	$S_y/(S_s\,H)$
κ_x, κ_z	$K_x/K_y,\ (K_z\,y_0^2)/(K_y\,H^2)$
κ_1, κ_2	$(K_1\,y_0)/(K_y\,b_1),\ (K_2\,y_0)/(K_y\,b_2)$
λ_0, λ_i	Roots of Eqs. (40) and (41), respectively
λ_s, λ_s'	$\sqrt{(\kappa_x\alpha_m^2+\beta_n^2)/\kappa_z},\ \beta_n/\sqrt{\kappa_z}$
$\mu_{n,0}$	Equaling $\mu_{m,n,0}$ defined in Eq. (36) with $\alpha_m = 0$
$\nu_{n,i}$	Equaling $\nu_{m,n,i}$ defined in Eq. (37) with $\alpha_m = 0$
θ_k	Counterclockwise angle from x axis to k-th lateral where $k \in (1, 2, \ldots N)$
$\max \bar{x}_k,\ \min \bar{x}_k$	Maximum and minimum of $\bar{x}_k$, respectively, where $k \in (1, 2, \ldots N)$

809

Figures

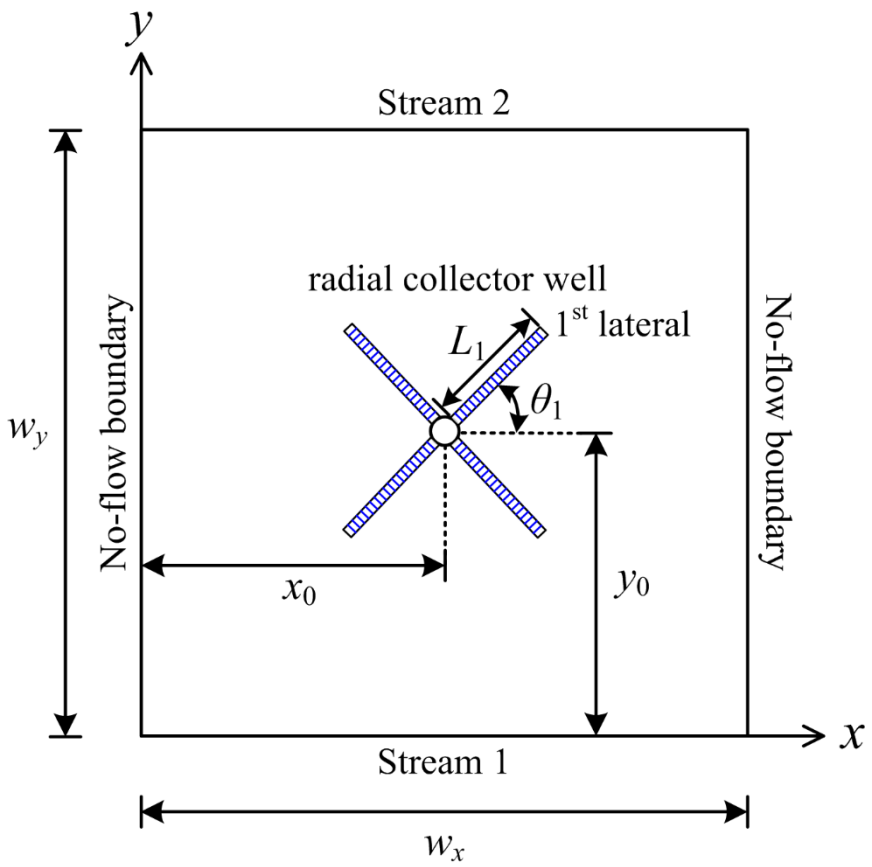

Figure 1. Schematic diagram of a radial collector well in a rectangular unconfined aquifer

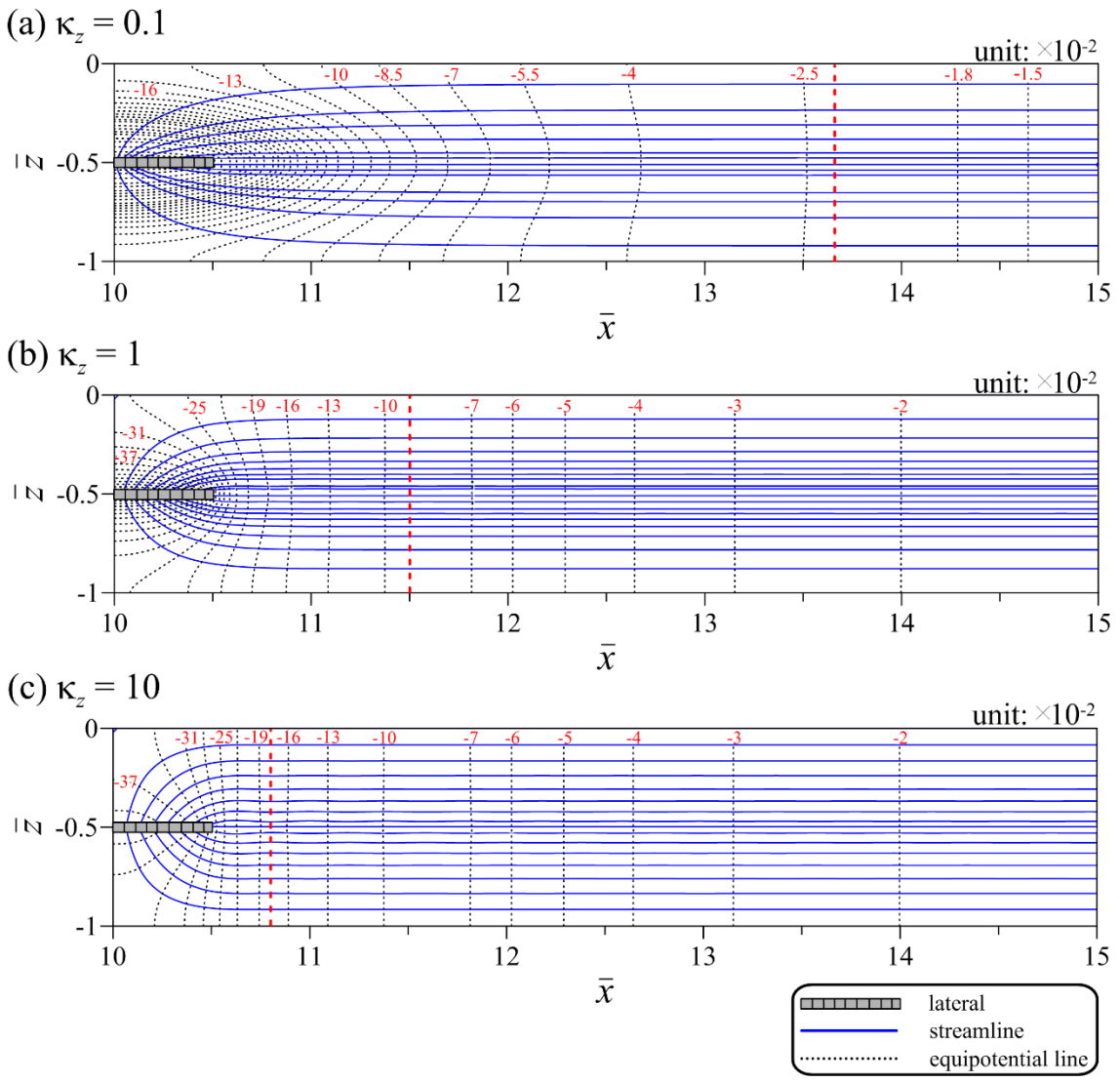

Figure 2. Streamlines and equipotential lines predicted by the present solution for κ_z = (a) 0.1, (b) 1 and (c) 10.

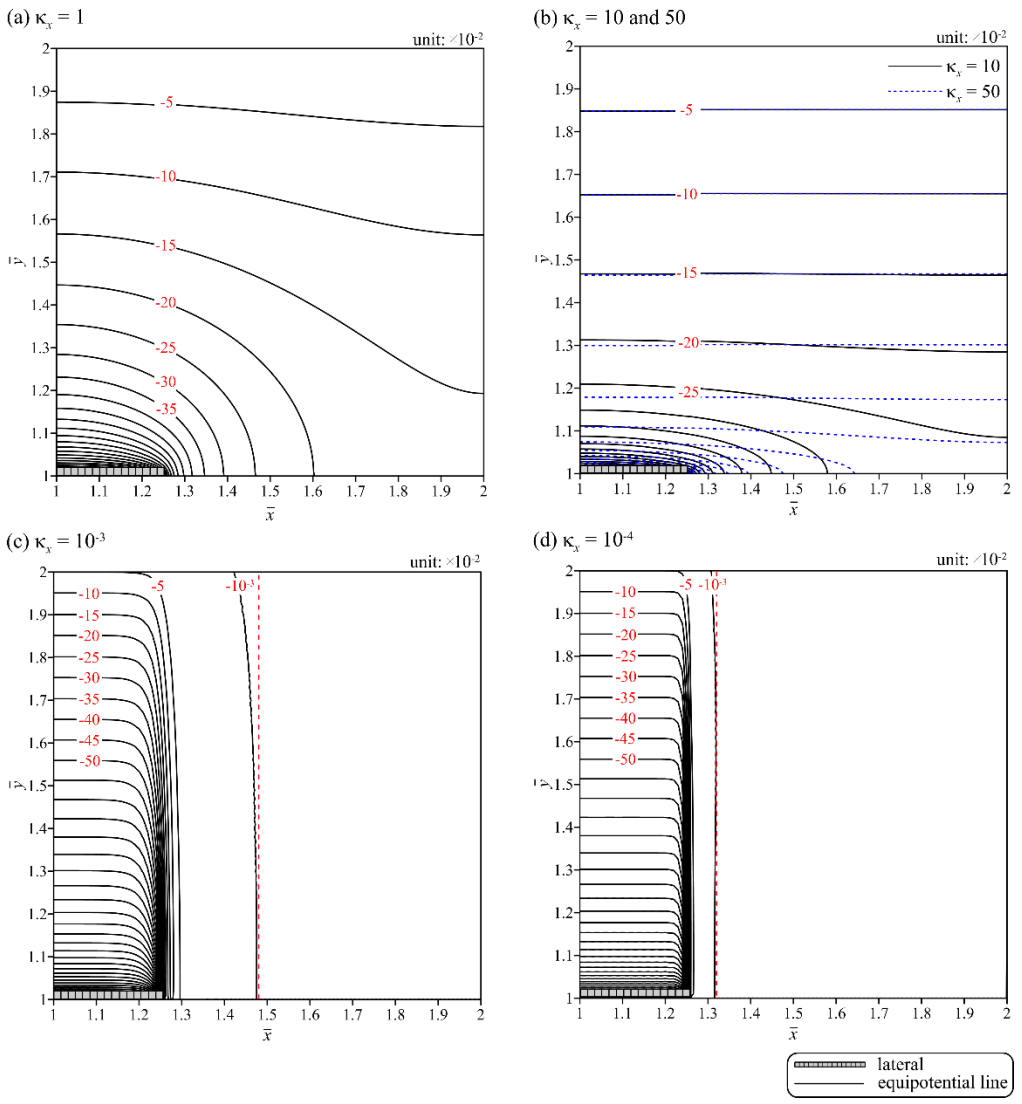

815

816 **Figure 3.** Spatial distributions of the dimensionless head predicted by the present head solution for κ_x = (a) 1, (b) 10 and 50, (c) 10^{-3} and (d) 10^{-4}.

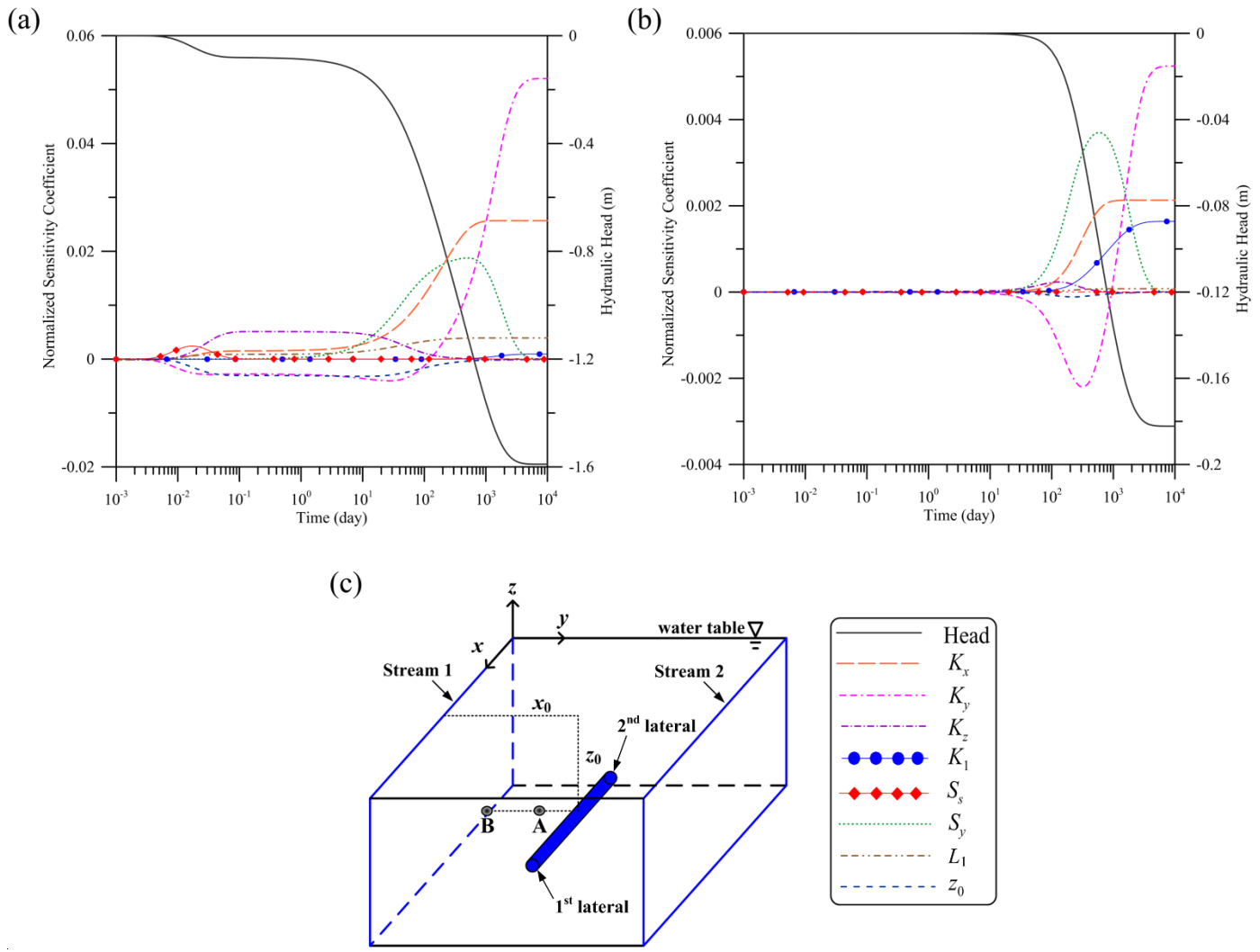

817

818 **Figure 4.** Temporal distribution curves of the normalized sensitivity coefficients for parameters K_x, K_y, K_z, S_s, S_y, K_1, L_1 and z_0 observed at
819 piezometers (a) A of (400 m, 340 m, −10 m) and (b) B of (400 m, 80 m, −10 m).

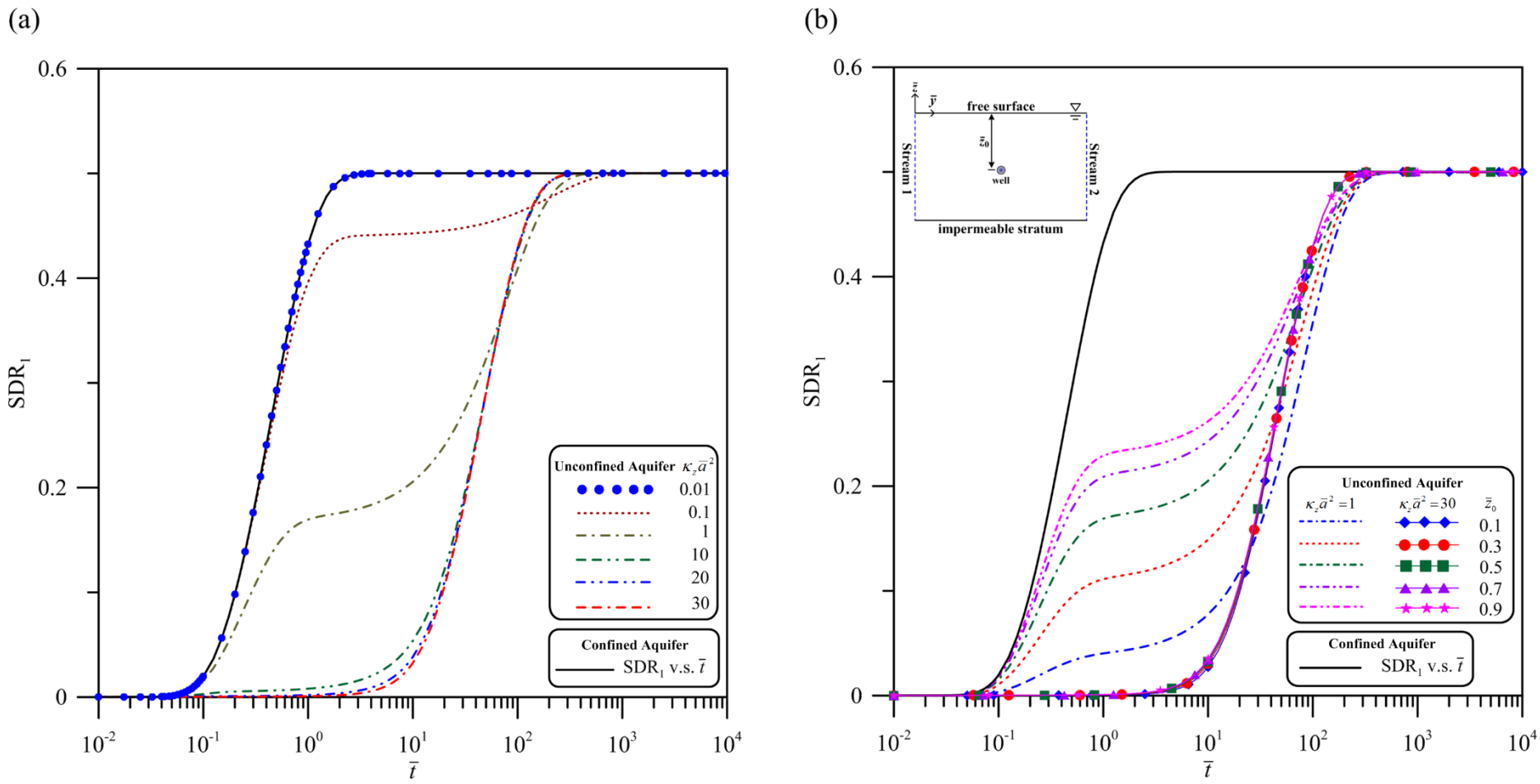

820

821 **Figure 5.** Temporal SDR_1 distributions predicted by Eq. (52) for stream 1 with various values of (a) $\kappa_z\bar{a}^2$ and (b) $\bar{z}_0$.

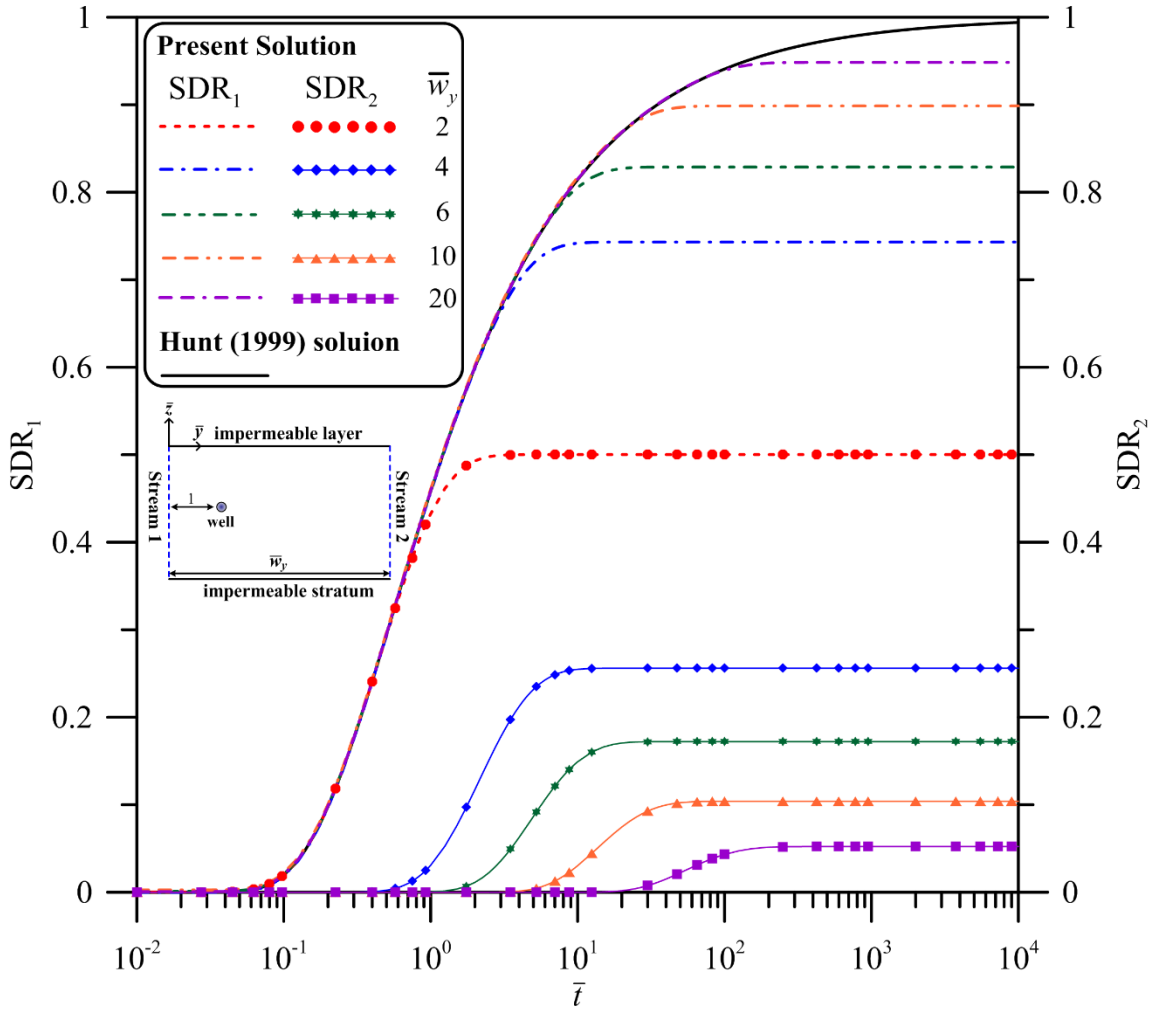

822

823 **Figure 6.** Temporal SDR distribution curves predicted by Eqs. (52) and (53) with $\gamma = 0$ for confined aquifers when $\overline{w}_y$ = 2, 4, 6, 10 and 20.